Investigation of MODIS snow cover products for use in streamflow prediction systems

by

Logan Ray Karsten

A thesis submitted to the graduate faculty

in partial fulfillment of the requirements for the degree of

MASTER OF SCIENCE

Major: Meteorology

Program of Study Committee:
Kristie J. Franz, Major Professor
William Gutowski
Brian K. Hornbuckle

Iowa State University

Ames, Iowa

2011

TABLE OF CONTENTS

LIST OF FIGURES

LIST OF TABLES

ABSTRACT

Many regions of the US rely on spring snow melt forecasts for water resource planning and flood prediction. With the potential for climate change to alter temperature and precipitation patterns during the cold season, snow information (both modeled and observed) will become increasingly important. Given limited snow and meteorological observations, the US National Weather Service streamflow forecasting system has relied on ground-based measurements of temperature and precipitation as input to a lumped, empirically-based snow model (the SNOW17) to track winter snowpack processes for decades. With the advent of satellite-based data sources and more powerful computing capabilities, the potential now exists to advance the forecasting system beyond this traditional modeling approach. Three possible areas of advancement in operational snow modeling are the use of: (1) a spatially distributed snow model, (2) direct input of satellite observations into the model, and (3) calibration of the snow model to satellite observations that are not available from ground-based monitoring sites or are unavailable at the watershed scale. The current study will investigate these three topics. We hypothesize that the application of snow data from the MODIS TERRA satellite, which provides spatially distributed hydrologic information in remote areas that are not generally monitored, will improve snow modeling for better spring streamflow predictions. Two different data applications were tested. First, the use of snow covered area data to calibrate the distributed SNOW17 model was investigated. Secondly, the application of MODIS snow albedo as input to an energy balance snow melt model was tested. The study area is the North Fork of the American River located in central California. The study period spans October 1st, 2000 through September 30th, 2009. Distributed

temperature and precipitation time series are created from station data and PRISM (Daly et al., 2010) using inverse distance weighting and application of hourly precipitation trends.

Results showed that a multi-step calibration approach using both remotely sensed snow cover information and stream flow discharge produced, on average, better streamflow simulations during the spring melt period than model parameters used in the operational system. In addition, the MODIS albedo appears to underestimate the snow surface albedo leading to erroneous early melting in the mode

CHAPTER 1: INTRODUCTION

1.1 Motivation and Overview

Snow melt plays an important role in the availability of water in many regions across the world. Worldwide, one-third or more of the water used for irrigation is produced from snow melt (Steppuhn, 1981). Within several alpine basins of the Rocky Mountains, up to 75% of annual precipitation falls as snow (Storr, 1967) and up to 90% of surface runoff is from snow melt (Goodell, 1966).

Operational snow forecasting plays a crucial role in water resource management in regions that are highly dependent on snow melt for hydrological resources. This is especially true under conditions of extreme (low or high) precipitation. For the Western U.S., climate change is bringing warmer temperatures during precipitation (Figure 1.1), resulting in decreasing snowpacks (Figure 1.2) (Stewart, 2009). A decrease in snowpack buildup during the winter time will translate into a loss of streamflow discharge later during the melt period. This change in timing could have impacts on water resource planning across these regions. According to Knowles et al. (2006), 75% of reporting stations across the west are showing a trend of decreasing snowfall in mountainous regions, leading to a decrease in stream discharge during spring. As climate patterns shift across these regions, spatial distribution of snow cover will change as well. Warmer climate patterns will alter patterns of snowfall accumulation and ablation to create new seasonal trends. This alteration may present a challenge to operational models that were developed using historical records from a different climate regime.

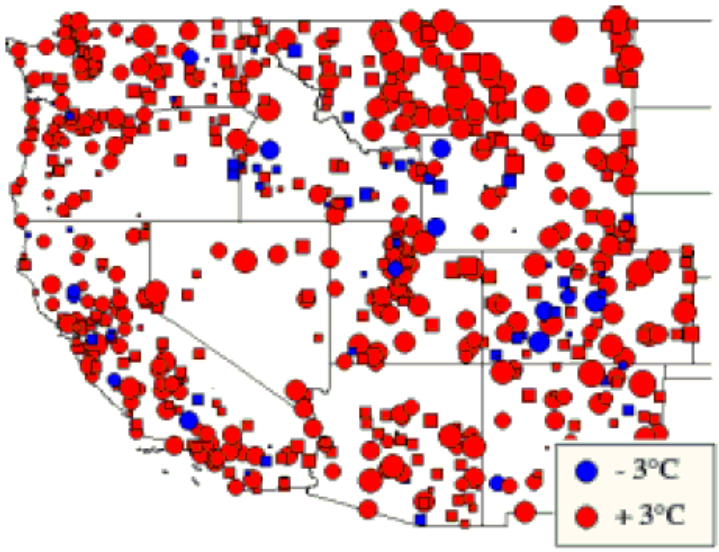

Figure 1.1: Trends in mean daily minimum temperatures during days of precipitation from 1949 to 2004. The symbol size is proportional to trend amounts. Circles indicate significant trends and squares indicate less significant trends. Source: Stewart (2009).

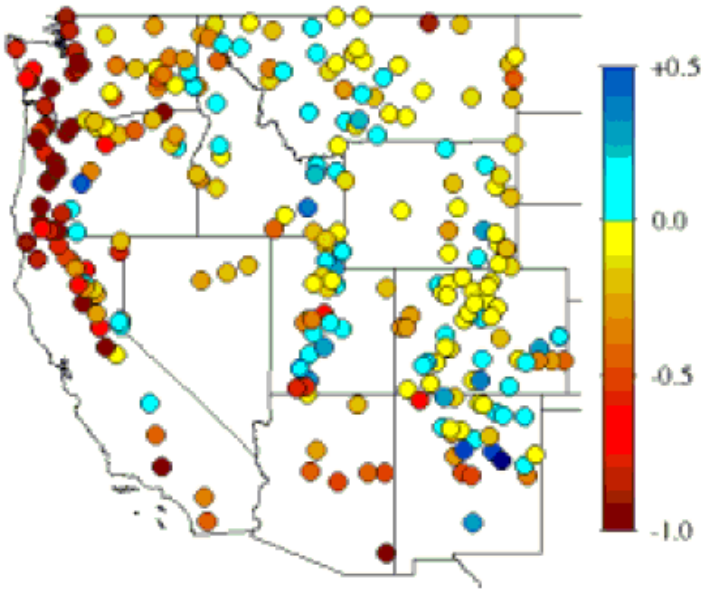

Figure 1.2: Trends in snowfall water equivalent, after removing trends of increasing or decreasing precipitation, from 1949 to 2004. Source: Stewart (2009).

While ground-based snow observations are available through an extensive network of snow courses and Snow TELemetry (SNOTEL) stations in the Western U.S. The Natural Resources Conservation Service (NRCS) operates more than 1,200 manually-measured snow courses, and over 750 automated SNOTEL stations in 13 states including Alaska. These sites are only representative of one specific point in a watershed. Therefore, in-situ observations can lead to the underestimation or overestimation of watershed-scale snowpack conditions due to highly variable spatial patterns of snow as a result of local vegetation or complex topography (Elder et al., 1991). Satellite remote sensing provides observations of surface variables in areas that are not covered by ground-based observations and has allowed for spatial measurement of snowpack properties, such as snow covered area (SCA).

Results from several recent studies suggest that remote sensing data has the potential to improve and advance operational snow and hydrological modeling applications. Andreadis and Lettenmaier, (2005) used the Ensemble Kalman Filter to assimilate snow cover extent information from the Moderate Imaging Spectroradiometer (MODIS) for four consecutive winters from 1999-2003. The data assimilation was used to update SCA in the variable infiltration capacity (VIC) macroscale hydrological model over the Snake River basin. By updating SCA, the model could make adjustments to SWE to reflect more realistic snow coverage patterns. The data assimilation technique successfully updated modeled snow cover area (SCA) to better agree with MODIS SCA and ground-based observations. Root mean square error (RMSE) for snow water equivalent (SWE), when validated against ground observations, decreased using the assimilation technique, especially for lower to middle elevations and periods of snow melt. Molotch and Bales (2006) evaluated the use of snow albedo derived from the Airborne Visible/Infrared Imaging Spectroradiometer (AVIRIS) in a

net radiation/temperature index snow melt model. The modeled SCA produced when using the AVIRIS-observed albedo data was compared to modeled SCA produced when using an age-decay function to estimate albedo. Results indicated that SCA was 79% more accurate when using the AVIRIS data when compared to on-site snow surveys.

Spatial snowpack information is particularly important for distributed snow modeling (as opposed to lumped snow modeling). With a lumped model, the watershed is treated as one system and the forcing data and parameters do not vary spatially. With a distributed model, the watershed is discretized into smaller sub-units, therefore spatial representations of forcing data and parameters are needed to accurately model the sub-watershed processes.

Two potential ways in which satellite data may support distributed modeling are: (1) through direct input of satellite observations into the snow model, and (2) calibration of the snow model to satellite observations that are not available from ground-based monitoring sites or are unavailable at the watershed scale. These topics are explored in this study using the National Weather Service (NWS) hydrologic prediction models: the SNOW17 empirically-based snowmelt model, (Anderson, 1973), and the Sacramento Soil Moisture Accounting (SACSMA) rainfall-runoff model (Burnash et al., 1973). A modified version of the SNOW17 (Franz et al., 2010) that introduces energy balance algorithms into the model structure is also tested. SCA and snow albedo from the Moderate Resolution Imaging Spectroradiometer (MODIS) Terra satellite are investigated for use with these models. The albedo data is tested as direct input into the Franz et al. 2010 model and the SCA is applied to model calibration.

A brief outline of the SNOW17 and SACSMA models and the MODIS data are given in the remainder of this introduction. The study methodology is presented in Chapter Two.

Results from various calibration techniques are presented in Chapter Three, and results from the albedo product testing are presented in Chapter Four. Implications of this study for operational forecasting and conclusions are discussed in Chapter Five.

1.2 SNOW17 Overview

The SNOW17 is a snow accumulation and ablation model used operationally by the NWS as part of the NWS River Forecasting System (NWSRFS). The model is based on empirical equations that use temperature to approximate energy exchange and melt within the snowpack. The only inputs into the model are air temperature and precipitation. The model accounts for changes in the heat content of the snowpack over time. When the snowpack is isothermal at 0 °C, additional heat energy (as measured by air temperature) will lead to melting of the snowpack. Below this point, the snowpack has a heat deficit which prevents melting and may lead to refreezing of any liquid water held within the snowpack.

The sequences of the SNOW17 model processes are shown in Figure 1.3. There are a total of 10 parameters that need to be defined for site specific conditions (Table 1.1). Four of the parameters are considered major in that they have the greatest impact on snowmelt computations (NWS, 2004). The remaining six are considered minor.

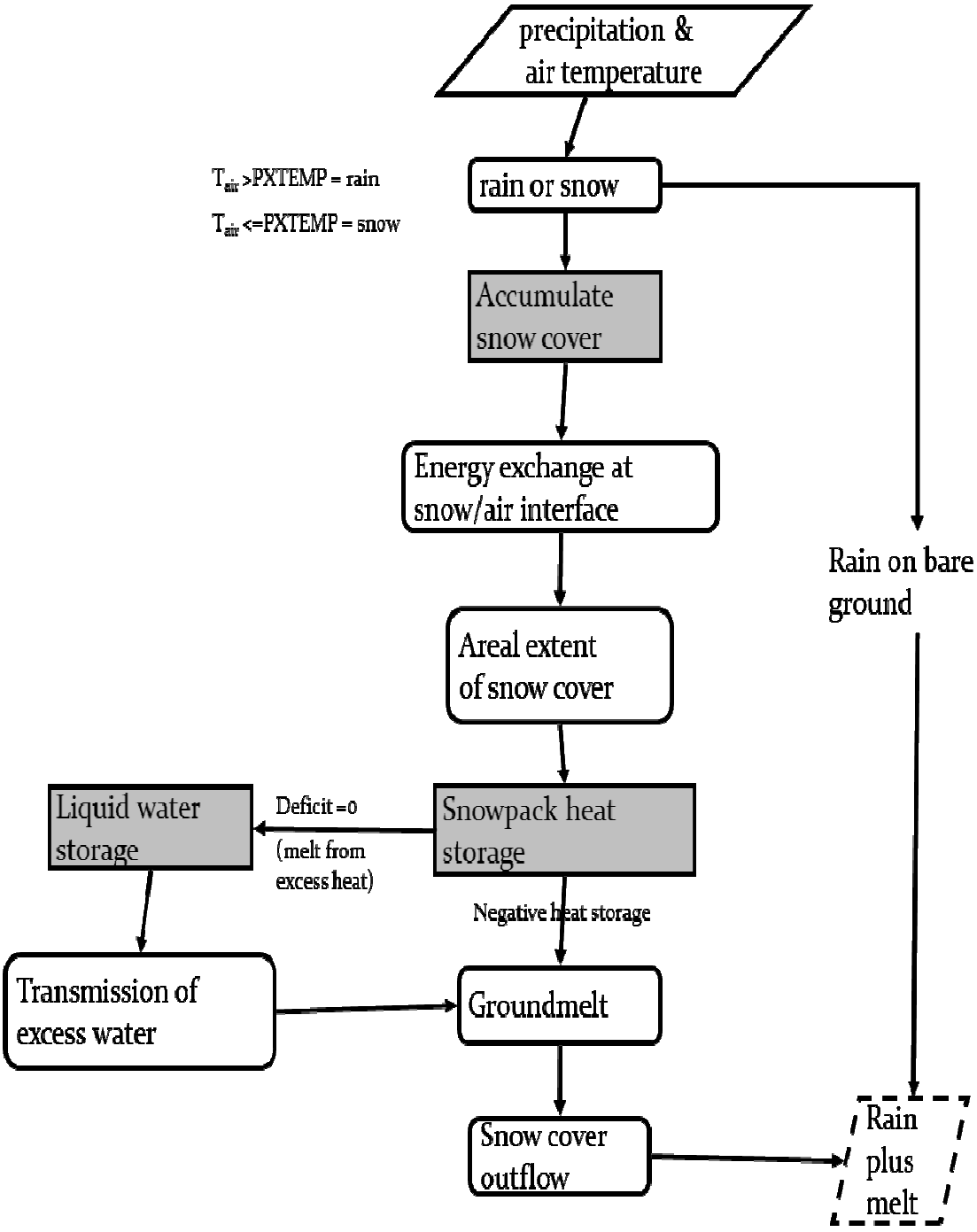

Figure 1.3 SNOW17 flow chart. Source: Franz (2006)

Table 1.1: SNOW17 parameters.

Parameter	Classification	Function
SCF	Major	A multiplying factor that adjusts the precipitation data and corrects for gage deficiencies. SCF also implicitly accounts for processes not included in the model that affects SWE, such as vapor transfer, interception, and drifting.
MFMAX	Major	Maximum melt factor during non-rain periods. (mm $°C^{-1}$ $6hr^{-1}$)
MFMIN	Major	Minimum melt factor during non-rain periods. (mm $°C^{-1}$ $6hr^{-1}$)
UADJ	Major	The average wind function during rain on snow events. (mm mb^{-1})
SI	Major	Depth of snow at which there is 100% snow cover. Below this value, areal depletion curves deplete SCA. (mm)
NMF	Minor	Maximum negative melt factor. (mm $°C^{-1}$ $6hr^{-1}$)
TIPM	Minor	Antecedent temperature index.
PXTEMP	Minor	Temperature that determines whether precipitation is rain/snow. (°C)
MBASE	Minor	Base temperature for snowmelt computations. (°C)
PLWHC	Minor	The maximum amount of liquid water that can be held in the snowpack.
DAYGM	Minor	Constant melt rate caused by the snow/soil interface. (mm)

1.3 Modified SNOW17

In addition to the operational SNOW17, a modified version of the model will be tested. This model incorporates physically-based energy balance processes and will allow data, such as albedo, to be applied for snow modeling which cannot be used in the original SNOW17. The major modification that was made is the replacement of the temperature index approach with a net radiation index approach of Brubaker et al. (1996) (Franz et al., 2010). An energy balance algorithm is used to track heat in the snow pack and to determine the amount of melt that will occur. In addition to temperature and precipitation, the modified model now requires incoming shortwave radiation at the surface, relative humidity, and wind speed. Relative humidity and air temperature are also used to estimate incoming long wave radiation. To calculate outgoing shortwave radiation, estimates of surface albedo are needed. Transitioning the model to a more physically-based approach resulted in the need for fewer

parameters, a total of six are required in the modified SNOW17 (Table 1.2) (Franz et al., 2010).

Table 1.2: Modified SNOW17 parameters

Parameter	Classification	Function
SCF	Major	A multiplying factor that adjusts the precipitation data and corrects for gage deficiencies. SCF also implicitly accounts for processes not included in the model that affects SWE, such as vapor transfer, interception, and drifting.
UADJ	Major	The average wind function during rain on snow events. (mm mb^{-1})
SI	Major	Depth of snow at which there is 100% snow cover. Below this value, areal depletion curves deplete SCA. (mm)
TIPM	Minor	Antecedent temperature index.
PXTEMP	Minor	Temperature that determines whether precipitation is rain/snow. (°C)
PLWHC	Minor	The maximum amount of liquid water that can be held in the snowpack.
DAYGM	Minor	Constant melt rate caused by the snow/soil interface. (mm)

1.4 SACSMA Overview

The Sacramento Soil Moisture Accounting (SACSMA) model (Burnash et al., 1973) is a conceptual, continuous rainfall runoff model used operationally by the NWS to forecast river discharge for watersheds across the U.S (Figure 1.4). This model incorporates several hydrological processes through a basic water balance equation of:

Runoff = Rainfall – Evapotranspiration – Changes in Soil Moisture

where all rainfall coming into the system must be utilized through evapotranspiration, storage in the watershed, leaving the watershed through channel flow, or leaving the watershed through subterranean drainage (Burnash et al., 1973). Changes in soil moisture are computed using a two-layer soil system. The upper soil layer accounts for surface soil conditions and interception-storage processes. The lower soil layer represents storage of deep soil moisture and ground-water (Brazil and Hudlow, 1981). Percolation of water from the upper layer to

the lower layer is dictated by gravitational forces and processes of evapotranspiration and infliltration. When precipitation exceeds percolation and interflow in the upper layer, saturation is reached and excess water exits the system as overland flow.

Inputs into the model include mean areal precipitation (mm) and potential evapotranspiration (mm). Outputs from the model are channel inflow (mm) and estimated evapotranspiration (mm). A unit-hydrograph, or other routing function, is used to convert the channel inflow to watershed discharge. Along with the unit-hydrograph, 16 parameter values need to be specified.

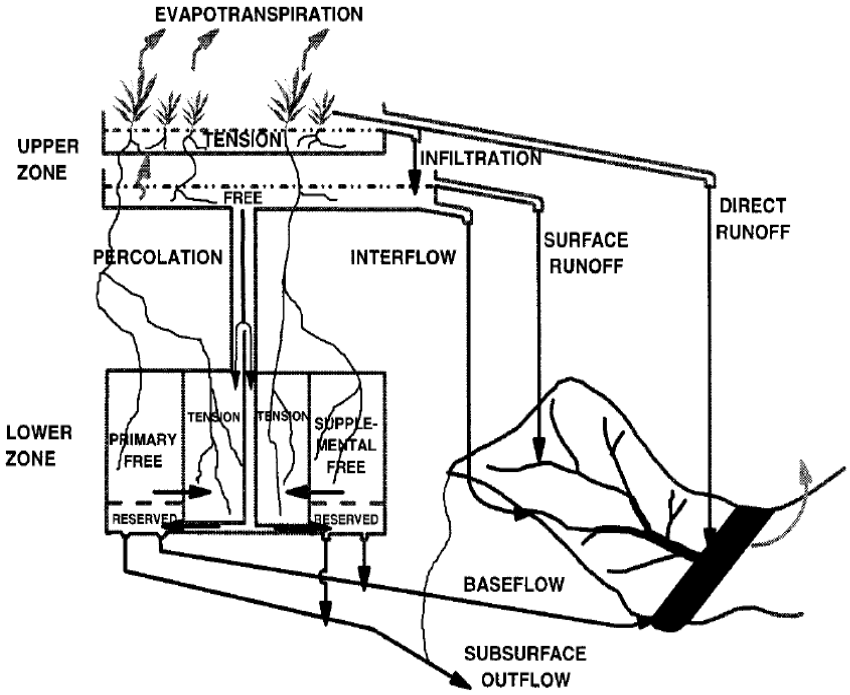

Figure 1.4: SACSMA flow chart. Source: Hogue et al. (2000)

1.5 MODIS Satellite Data

The Moderate Resolution Imaging Spectroradiometer (MODIS) is aboard two satellites, AQUA and TERRA. The TERRA satellite was launched in 1999, and AQUA was launched in 2002. Both satellites are in geo-synchronized orbits around the Earth. They serve as part of NASA's Earth Observing System, which is designed to collect important remote sensing data of Earth's atmosphere and land surface. MODIS collects data in 36 spectral bands at various wavelengths using passive remote sensing. Two snow products that MODIS offers with potential relevance to operational forecasting are SCA and snow albedo.

MODIS SCA products have been shown to be a reliable source of spatial snow cover information in several studies. A study by Bitner et al. (2002) compared maps of SCA generated from the National Operational Hydrologic Remote Sensing Center, and SCA generated from MODIS. The study showed MODIS and NOHRSC products to be equal 94% of the time in the Pacific Northwest and 95% of the time in the Great Plains. However, it should be noted that NOHRSC SCA analysis is generated using data assimilation of observations and airborne snow surveys. Another study done by Dery et al. (2005) derived snow areal depletion curves from MODIS SCA and utilized them in the parameterization of a catchment-based land surface model. The authors of this study showed that with the MODIS-derived areal depletion curves, the mean absolute error of the model was reduced from 0.65 mm per day to 0.48 mm per day. In addition, Dery et al. (2005) compared MODIS SCA to the Landsat SCA and found that for values of 20% to 100% snow covered area, there were differences of only 5% in the MODIS SCA. However, during periods when snow covered area values were less than 20%, the differences increased up to 13%.

Maurer et al. (2003) validated MODIS SCA to ground-based observations and compared the results data from the NOHRSC SCA. They found that the MODIS SCA misclassified up to 5% fewer pixel cells compared to the NOHRSC SCA. A similar study done by Klein and Barnett (2003) validated MODIS SCA against ground-based observations and also compared the MODIS and NOHRSC SCA. This comparison was done over the Upper Rio Grande River Basin in Colorado. Results showed that MODIS data was accurate 94% of the time while NOHRSC was accurate 76% of the time. Based on these series of studies, MODIS SCA shows promise for use in SNOW17 model applications, such as model calibration.

In addition to snow covered area, studies have shown snow albedo from the MODIS satellite provides accurate snow information with the potential for model applications. A study done by Tekeli et al. (2006) compared a group of surface-based albedo observations to MODIS snow albedo values and found the satellite values to be within 10% of the in-situ values. Another study done by Stroeve et al. (2006) validated MODIS snow albedo to ground-based measurements and found a root-mean-square error of 0.067, which translates to a RMSE error of less than 10% snow albedo. An intensive field campaign done by Klein (2003) compared broadband snow albedo retrieved from several in-situ sites located within a MODIS pixel cell to MODIS albedo values. The study found that the in-situ values were within 10% of the MODIS values during the period of study.

At this time, the snow albedo products available through the MODIS dataset are still in an experimental stage of development. Despite the apparent accuracy of MODIS snow albedo shown in prior studies, the accuracy of snow surface albedo from MODIS in heavily forested regions may be questionable. The snow albedo prototype algorithm developed by Klein and Stroeve (2002), and shown in Figure 1.5, uses a bidirectional reflectance

distribution function (BRDF) for non-forested regions. This is done to account for anisotropic scattering associated with snow-covered surfaces. However, the BRDF function does not work for surfaces covered with dense tree canopies. Therefore, the snow surface is treated as Lambertian. With a Lambertian surface, the brightness temperature of the surface will be the same regardless of angle of observation. For a heavily forested region, radiation leaving the surface of the snow pack will encounter numerous trees, altering the brightness temperature for all angles of viewing. This presents a challenge because a dense tree canopy will hinder the satellite's ability to accurately remotely-sense the snow surface. Nonetheless, limited ground-based observations make satellite the only viable source of surface albedo information.

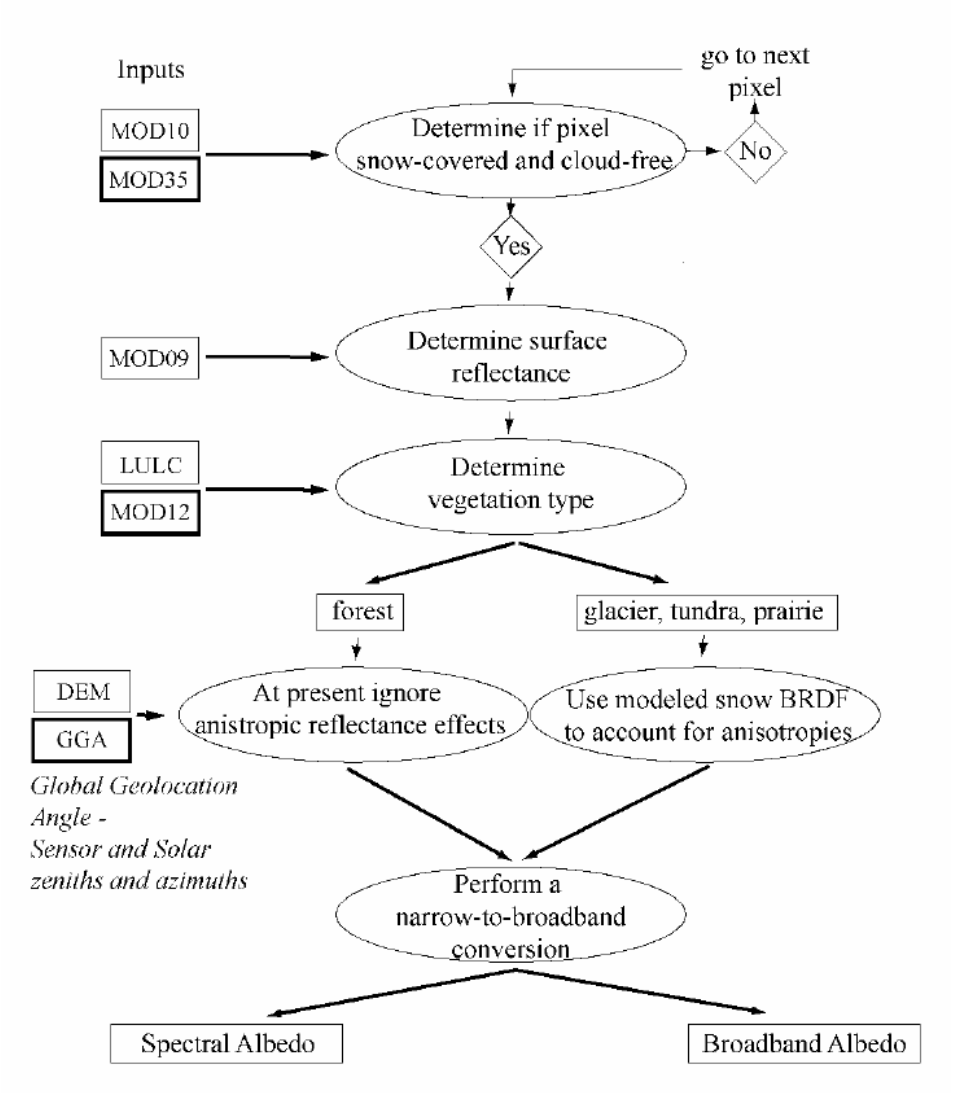

Figure 1.5: Formulation of MODIS snow albedo. Source: Klein and Stroeve (2002).

CHAPTER 2: METHODOLOGY

2.1 Study Area

The study area is the North Fork of the American River basin, located within the Sierra Nevada Mountains in California (Figure 2.1). The watershed area is 1109 km^2, and has a range of elevation from 182 meters to 2714 meters. The region that contains the drainage area stretches from latitude 38.6° to 39.4° and from longitude 121.2° to 120.2°. The North Fork River drains from the Sierra Nevada mountain range and merges with the Middle and South Fork of the American River. The eventual path of the American River leads to Folsom Lake, which serves as a reservoir for flood mitigation, water resources management, and hydroelectric power for the Sacramento area (Dettinger et al., 2004). The watershed is mostly undeveloped. The vegetation consists of mostly pine-oak woodlands and rangelands (Dettinger et al., 2004). The outlet of the study area is a United States Geological Survey stream site 11427000 located at latitude 38°56’10” and longitude 121°01’22”.

Precipitation that falls during the winter falls as either rain or snow, depending on meteorological conditions, while summers tend to be hot and dry for the majority of the region. Above 1500 meters, much of the winter time precipitation falls as snow, aiding in the development of a deep snow pack. In lower elevations, the precipitation type can vary depending on the temperature. There is also a large variability of precipitation amounts with elevation. Upper elevations can see as much as 1800 mm of precipitation while lower elevations may not see any more than 450 mm (Shamir and Georgakakos, 2006). Several recent climate studies acknowledge the potential for significant changes in hydrological patterns for this region over the next several decades (Miller et al., 2003; Wilby and Dettinger, 2003; Dettinger et al., 2004).

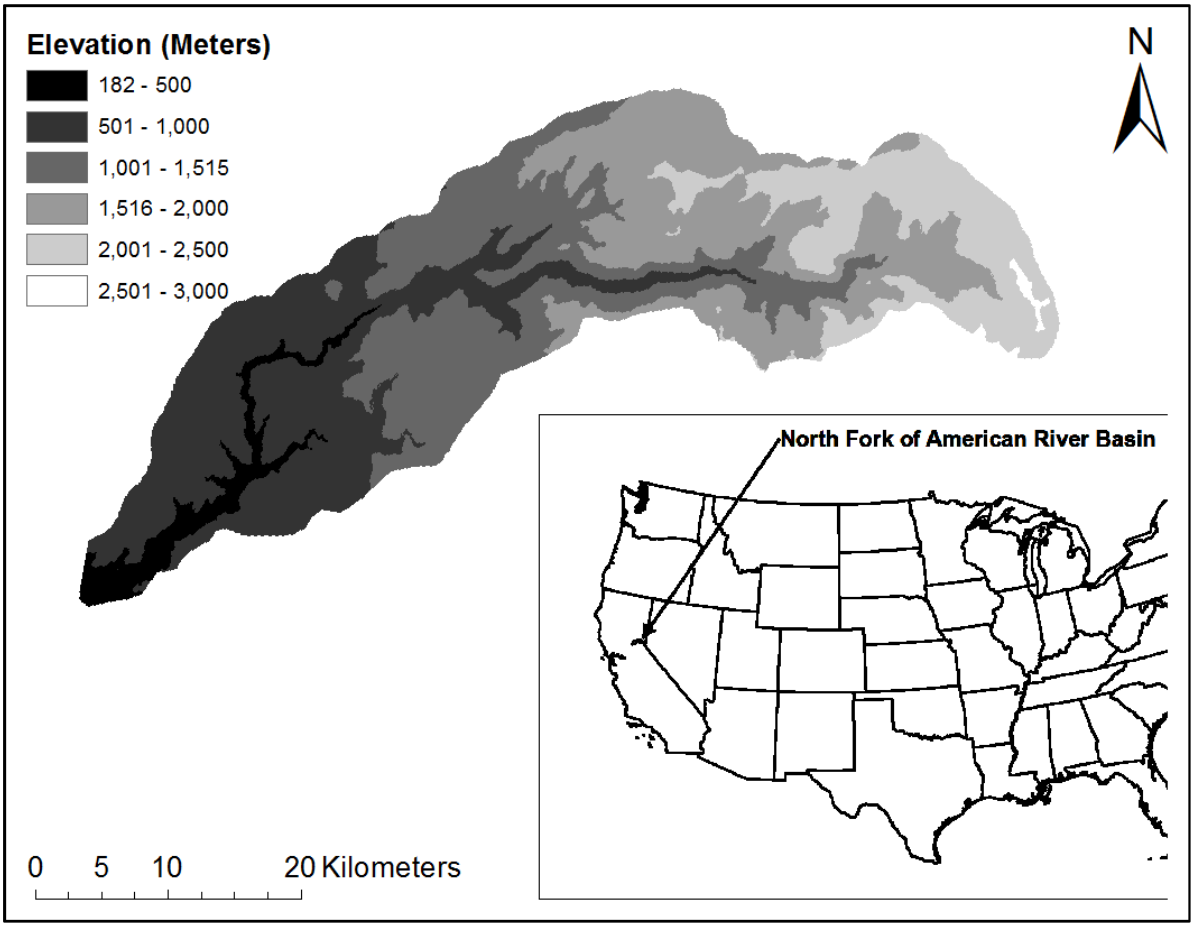

Figure 2.1: Layout of North Fork of American River Basin located in the Sierra Nevada, CA.

2.2 Data

Forcing data to be used in the models were prepared using both ground-based observations and reanalysis data. The study period spans from October 1st, 2000 through September 30th, 2009. Data was processed for every six hours beginning at 0000 UTC. The steps that were used to process the data are explained in the following sections. All data was prepared at a 1 km resolution over a domain that contained the study area, which was 9,434 km^2. The projection used for all data was the Universal Transverse Mercator (UTM)

projection. An associated Digital Elevation Model (DEM) was created using 1/3 arc-second elevation data, in meters, provided by the USGS Seamless Server (http://seamless.usgs.gov/). The 1/3 arc-second elevation data was re-projected into a 1 km UTM resolution using GIS and the domain boundaries. In addition, a watershed outline of the North Fork of the American River Basin was obtained from the Environmental Protection Agency (EPA; http://www.epa.gov/waterscience/ftp/basins/gis_data/huc/). This outline was used in the models to classify each pixel cell as either within the watershed or outside the watershed.

2.2.1 Temperature

Temperature data (°C) were obtained from in-situ ground observations within and around the watershed. Two sets of ground-based observations were chosen for this study. The first set was provided through the California Data Exchange Center (CDEC; http://cdec.water.ca.gov/), which is part of the California Department of Water Resources. The CDEC installs, maintains, and operates an extensive hydrologic data collection network including temperature and precipitation sensors. The CDEC operates and maintains 211 stations that relay observations to federal, state and other agencies via an automated data exchange program. For this study, 39 stations (within and near the domain study area) from the CDEC were chosen to be used in processing (Table 2.1).

Temperature data from the National Weather Service (NWS) Cooperative Observer Program (COOP) was also used. The COOP is a network of observers across the U.S. providing voluntary meteorological information. For this study, 24 stations (within and near the domain study area) were chosen to generate a temperature data set (Table 2.2). Unlike the CDEC stations, the COOP data collected was daily maximum and minimum temperature

values. Average daily temperature trends were generated from the hourly CDEC stations and applied to the daily COOP data to generate hourly temperature values for each COOP station.

Using GIS, inverse distance weighting (IDW) was applied to both CDEC and COOP temperature values for each time step to create a spatially interpolated data set. During the interpolation, any site that had missing data was ignored. Using GIS, the spatial data set was then re-projected into the UTM 1 km resolution used for the DEM. A 1 km temperature data set was extracted for each time step for the domain of the DEM.

Table 2.1: CDEC stations chosen for temperature data for the 2000 through 2008 water years.

Site	Elevation (ft)	Longitude	Latitude
ADR	1,200	121.0450° West	38.8820° North
ALP	7,600	120.2150° West	38.8050° North
BGR	800	121.3861° West	39.3808° North
BLC	5,280	120.7080° West	39.2760° North
BLK	8,000	119.9310° West	38.6130° North
BLT	1,138	121.0170° West	38.5860° North
BMT	4,680	120.6830° West	38.9000° North
CAP	8,000	120.0420° West	38.7100° North
FLL	6,250	120.0560° West	38.9320° North
GKS	5,600	120.5580° West	39.0750° North
GRZ	6,900	120.6450° West	39.9170° North
GTW	3,250	120.7890° West	38.9250° North
HGM	8,000	119.9400° West	38.8530° North
HLH	4,580	120.4217° West	39.0717° North
HVN	8,800	119.9170° West	38.9290° North
HYS	6,600	120.5270° West	39.2820° North
IDC	7,000	120.2990° West	39.4540° North
IDP	8,450	120.3220° West	39.4350° North
INN	6,500	120.2930° West	39.4940° North
LCN	200	121.2720° West	38.8820° North
LOS	8,600	120.1970° West	38.9250° North
MDL	7,900	120.1400° West	38.6150° North
MDW	7,200	120.5080° West	39.4170° North
OWC	4,500	120.2450° West	38.7330° North
PFH	3,440	120.5000° West	38.7600° North

Table 2.1 Continued

PKC	3,714	121.2020° West	39.4750° North
QCY	3,408	120.9500° West	39.9350° North
QYR	3,500	120.9410° West	39.9750° North
RBP	5,150	120.3750° West	38.9030° North
RP2	7,500	120.1400° West	39.0010° North
SCN	8,750	120.0680° West	38.7470° North
SGP	3,843	120.7500° West	39.1280° North
SLP	3,530	120.5630° West	38.7180° North
SQV	8,200	120.2760° West	39.1940° North
SRT	2,720	120.8830° West	39.1830° North
TK2	6,400	120.1940° West	39.3000° North
VVL	6,700	120.3050° West	38.9450° North
WC3	6,750	120.2200° West	39.1370° North
BKD	1,600	121.8840° West	37.9500° North

Table 2.2: COOP stations chosen for both temperature and precipitation data for the 2000 through 2008 water years.

Site	Elevation (ft)	Longitude	Latitude
040931	5,575	120.10° West	39.38° North
41018	5,385	120.65° West	39.45° North
41072	6,470	119.23° West	38.25° North
41277	4,695	120.32° West	38.28° North
41428	658	120.85° West	38.25° North
41912	2,380	120.95° West	39.08° North
41948	50	122.03° West	39.18° North
42500	2,915	120.82° West	39.57° North
43573	2,400	121.07° West	39.20° North
45032	40	121.28° West	38.10° North
46136	2,781	121.00° West	39.25° North
46521	171	121.55° West	39.52° North
46960	1,890	120.82° West	38.70° North
47633	38	121.42° West	38.55° North
48606	3,808	121.10° West	39.57° North
48758	6,230	120.15° West	39.17° North
48762	6,314	120.00° West	38.90° North
262119	7,334	119.88° West	38.98° North
265191	4,709	119.78° West	39.95° North
268186	5,105	119.52° West	38.73° North

Table 2.2 Continued

267953	3,900	119.58° West	39.95° North
263090	3,956	119.20° West	40.38° North
262780	3,965	118.76° West	39.45° North
267612	5,000	119.35° West	38.86° North

2.2.2 Precipitation

The steps involved in generating a precipitation (mm) data set were slightly different than for the temperature data. Only one set of ground-based precipitation observations were collected. Table 2.3 lists the 39 CDEC stations that were chosen for hourly precipitation data. Subjective analysis of the CDEC ground observations showed that precipitation trends were representative of true conditions. However, the magnitudes of precipitation values were determined to be too large. This lead to a conclusion that data from the CDEC stations were insufficient to generate a reliable spatial precipitation data set. Because the hourly precipitation trends were found to be representative of true conditions, six-hourly precipitation trends were extracted from the CDEC. This was done by calculating what percentage of monthly total precipitation fell over a six-hour time period. These trends will be applied in the next step of data processing for precipitation.

A second set of precipitation data was downloaded from the Parameter-elevation Regressions on Independent Slopes Model (PRISM) website (http://www.prism.oregonstate.edu/) hosted by Oregon State University. PRISM is a knowledge-based system that uses point measurements of precipitation, temperature, and other climatic factors to produce continuous, digital grid estimates of monthly, yearly, and event-based climatic parameters (Daly et al., 2010). In addition, the data is continuously

updated, incorporating point data, a digital elevation model, and knowledge of climatic extremes, such as rain shadows, coastal effects, and temperature inversions (Daly et al., 2010).

One of the products offered by PRISM is monthly total precipitation over the U.S. The data was collected for the entire period of study at 2.5 arcmin, or about 4 km resolution.

The six-hour temperature trends extracted from the CDEC data were applied to the monthly PRISM data to produce the six-hour spatial precipitation data set needed for this study. The precipitation data was then re-projected into a UTM 1 km resolution to match the precipitation and DEM projection using GIS.

Table 2.3: CDEC stations chosen for precipitation data for 2000 through 2008 water years.

Site	Elevation (ft)	Longitude	Latitude
FRD	5,517	120.1830° West	39.8830° North
SPL	6,867	120.0540° West	39.4830° North
INN	6,500	120.2930° West	39.4940° North
SBY	3,810	121.1060° West	39.5640° North
FBS	2,840	121.2661° West	39.5170° North
BGR	800	121.3861° West	39.3808° North
PKC	3,714	121.2020° West	39.4750° North
ENG	551	121.2670° West	39.2390° North
CAM	2,755	121.0490° West	39.4510° North
ALY	4,957	120.8750° West	39.4700° North
WTC	4,321	120.8375° West	39.3167° North
DPH	3,400	120.7670° West	39.2640° North
IDP	8,450	120.3220° West	39.4350° North
IDC	7,000	120.2990° West	39.4540° North
TK2	6,400	120.1940° West	39.3000° North
MRT	5,745	120.1130° West	39.3270° North
STP	5,956	120.1030° West	39.4710° North
TCC	6,750	120.1540° West	39.1720° North
SQV	8,200	120.2760° West	39.1940° North
RP2	7,500	120.1400° West	39.0010° North
HLH	4,580	120.4217° West	39.0717° North

Table 2.3 Continued

SRT	2,720	120.8830° West	39.1830° North
LCN	200	121.2720° West	38.8820° North
PIH	1,200	121.0092° West	38.8317° North
BMT	4,680	120.6830° West	38.9000° North
VVL	6,700	120.3050° West	38.9450° North
RBB	5,900	120.3780° West	38.9120° North
RBP	5,150	120.3750° West	38.9030° North
OWC	4,500	120.2450° West	38.7330° North
BTA	7,600	120.2000° West	38.8000° North
SCN	8,750	120.0680° West	38.7470° North
FLL	6,250	120.0560° West	38.9320° North
HGM	8,000	119.9400° West	38.8530° North
HVN	8,800	119.9170° West	38.9290° North
BLK	8,000	119.9310° West	38.6130° North
SIL	7,100	120.1180° West	38.6780° North
MDL	7,900	120.1400° West	38.6150° North
BLT	1,138	121.0170° West	38.5860° North
BKD	1,600	121.8840° West	37.9500° North

2.2.3 Incoming Shortwave Radiation

The North American Regional Reanalysis (NARR) data set provided by the National Oceanic and Atmospheric Administration (NOAA) was used to develop an incoming shortwave radiation time series (Messinger et al., 2005). The NARR is a long-term climate data set covering the North American continent spanning back to 1979. The data was produced using the ETA/NOAH Land-Surface Model and data assimilation at a 32 km resolution. Data is available for 45 layers of the atmosphere, including the land surface. In addition, the data is offered at a three hour timestep starting at 0000 UTC (Messinger et al., 2005).

NARR data was obtained for the period of study. The incoming shortwave radiation variable (W/m^2) was extracted and re-projected into a UTM 1 km resolution using GIS.

Due to the large resolution of the NARR data set, further downscaling of incoming shortwave radiation was desired to obtain a data set that was more representative of 1 km resolution. To do this, downscaling was done by based on local topography. Using the aforementioned DEM and GIS, incoming clear sky radiation was calculated for every three hours throughout the year at the UTM 1 km resolution. This was done to account for topography at the 1 km scale. Next, incoming clear sky shortwave radiation was calculated for a flat surface at the same latitude at the same temporal resolution. From these two sets of incoming clear sky radiation, a ratio of incoming clear sky radiation with topography to incoming clear sky radiation on a flat surface was calculated. For the next step, the assumption was made that incoming shortwave radiation at the 32 km resolution is broad enough to be treated as a flat surface. It was also assumed that local effects of backscattering and atmospheric effects were already accounted for by the NARR data set. The ratio was then applied to the NARR incoming shortwave radiation to generate a topographically corrected incoming shortwave radiation data set at every three hours. The ratio was applied for every time step to produce a topographically corrected incoming shortwave radiation data set. To produce data for every six hours, two sets of three-hour data sets were averaged together to produce a six-hour average of incoming shortwave radiation reaching the surface.

2.2.4 Relative Humidity

Relative humidity was prepared in a similar manner as the incoming shortwave radiation data. Relative humidity at the surface was extracted from the NARR files for every three hours. The data was re-projected into a UTM 1 km resolution using GIS. To produce data for every six hours, two sets of three-hour data sets were averaged together to produce a

six-hour average of surface relative humidity. No downscaling was applied to the relative humidity.

2.2.5 MODIS Snow Products

MODIS satellite data was collected for the study period via FTP from the National Aeronautics and Space Administration (NASA; ftp://n4ftl01u.ecs.nasa.gov/SAN/MOST/). All snow products were collected from the Terra satellite, which are MOD10A1 files. Snow products are offered as a daily average on a 500-m grid. Using latitude and longitude coordinates of the study domain, the satellite data was aggregated to a 1 km resolution with an area matching the other forcing data. This was done by taking the average latitude and longitude values for each 1 km grid cell and assigning the MODIS value from that latitude and longitude point to the grid cell.

Missing data occur due to cloud cover during the time of observation, and within the MODIS data set these periods are classified as missing due to cloud cover. Linear interpolation between available time periods was performed to create a complete data set. This was done for both the SCA and snow albedo product for the entire period of study.

2.3 Calibration

The Shuffled Complex Evolution Algorithm (SCE-UA) (Duan et al., 1993) was used to automatically calibrate key parameters for both the SNOW17 and the SACSMA models for the North Fork of American River basin. The SCE-UA is an automatic calibration method developed in response to the limitations of previous automatic calibration methods which often found local optimum parameter sets rather than global optimum parameter sets. Water

years 2001-2004 were used for the calibration period, and water years 2005-2009 were used for verification. Calibration was conducted using mean absolute error (MAE) as the objective function:

$$\text{MAE} = \frac{1}{n}\sum_{t=1}^{n}|d_t - o_t| \quad (2.1)$$

Where d_t is modeled discharge, o_t is observed discharge, and n is the number of pixel cells.

In mountainous regions, the NWS forecasters will divide the watershed into elevation zones (generally two or three), run the forecast models for each zone, then aggregate the results to get watershed outflow. This is done to account for variations in the amount of snowfall received across elevation zones, where lower elevations generally have little snowfall and the highest elevations have the highest snowfall. The California Nevada River Forecast Center (CNRFC) uses historical data sets to calibrate the SNOW17 parameters for the lower and upper elevation zones (Table 2.4). Traditionally, the operational models are calibrated using watershed discharge, rather than snow observations, as the optimization variable.

Following the practice of CNRFC, in this study the assumption is made that parameters are a function of elevation as a result of the variation in climate. To account for both climate and possible parameter variability with elevation, the watershed was divided into six different elevation zones for the SNOW17 model (Table 2.5). Within each elevation zone, the SNOW17 parameters are lumped, or set to the same value. Although parameters are lumped by elevation zone, note that the model is still run at a 1 km grid scale.

The CNRFC calibrates the SACSMA in a similar manner as the SNOW17, producing separate calibrated parameter sets for the upper and lower elevation zones (Table 2.7), the

SACSMA model is applied using the two elevation zones defined by the NWS for the North Fork of the American basin (Table 2.6) rather than the six zones as described in the previous paragraph. In the model application presented here, the lower three elevation zones of the SNOW17 encompass the lower elevation zone of the SACSMA, and the top three elevation zones for the SNOW17 encompass the upper elevation zone of the SACSMA. To generate discharge simulations, the SNOW17 output from the upper (lower) three elevation zones are aggregated and input into the upper (lower) SAC model. The combined runoff from both SAC elevation zones is routed to the basin outlet to compute discharge.

Table 2.4: CNRFC SNOW17 parameter values.

Parameter	Lower Elevation Zone	Upper Elevation Zone
SCF	1.1	1.2
MFMAX	0.95	0.90
MFMIN	0.08	0.07
UADJ	0.08	0.12
SI	409	1600
NMF	0.15	0.15
TIPM	0.25	0.25
MBASE	0.0	0.0
PXTEMP	1.5	1.5
PLWHC	0.12	0.02
DAYGM	0.3	0.3

Table 2.5: Elevation zones for SNOW17.

Elevation Zone	Lower Elevation Bound (Meters)	Upper Elevation Bound (Meters)
1	1	500
2	501	1000
3	1001	1515
4	1516	2000
5	2001	2500
6	2501	3000

Table 2.6: Elevation Zones for SACSMA.

Elevation Zone	Lower Elevation Bound (Meters)	Upper Elevation Bound (Meters)
1	1	1515
2	1516	3000

Table 2.7: CNRFC SACSMA parameter values.

Parameter	Lower Elevation Zone	Upper Elevation Zone
UZTWM	155	145
UZFWM	50	50
UZK	0.15	0.25
ADIMP	0.0	0.25
PCTIM	0.008	0.005
K	0.10937	0.10937
ZPERC	9.0	12.0
REXP	1.1	1.05
LZTWM	310	250
LZFSM	90	130
LZFPM	70	210
LZSK	0.1	0.08
LZPK	0.004	0.002
PFREE	0.2	0.30
RSERV	0.3	0.30
SIDE	0.0	0.0
PXMLT	1.0	1.0
RIVA	0.01	0.01

The SNOW17 was calibrated in multiple steps, and optimization of different combinations of parameters during calibration was tested. In the first calibration, three of the ten SNOW17 parameters (SI, MFMAX, PXTEMP) were calibrated using MODIS SCA. All other parameters were set to the values used by the CNRFC in the operational forecasting system. Each elevation zone was calibrated one at a time. MAE was calculated as the

difference between modeled SCA and observed MODIS SCA at each pixel and then averaged across the elevation zone for evaluating the convergence criteria.

SI is a threshold value below which less than 100% SCA is assumed. If the modeled snow water equivalent (SWE) is below this value, a SNOW17 areal depletion curve is used to estimate the SCA. Therefore, the parameter SI should be sensitive to the optimization routine when using MODIS SCA. MFMAX was chosen for calibration because it has the greatest influence on the melting process that occurs during the spring melt period, compared to the other melt factor parameter, MFMIN. Because SCA is computed based on modeled SWE, and therefore modeled melt varying MFMAX values can have an impact on SCA values during the melt period. PXTEMP was chosen because it determines whether precipitation occurs as rain or snow, and therefore determines the accumulation of snow cover. Even during the melt period this can be an important parameter. Even after snow cover begins to deplete, SCA will be reset to 100% in the model if a new snowfall occurs. Therefore, PXTEMP can play a significant role in the buildup or depletion of SCA, especially for the lower elevation zones. The SI, MFMAX and PXTEMP parameter values calibrated during this calibration will be used in the second calibration and held constant.

For the second calibration, the SCF parameter for the SNOW17 was calibrated. The MAE objective function was again used. In this test, the SNOW17 was run in conjunction with the SACSMA model and the parameter value was calibrated for each elevation zone using modeled discharge. The SACSMA parameters were not calibrated, rather the operational SACSMA parameters used by the CNRFC for the upper and lower half of the watershed were used. As in the previous steps, all SNOW17 parameters not calibrated in this study were also taken from the CNRFC operational system. Because the SCF is a correction

factor used to adjust the amount of snowfall in the SNOW17, this calibration optimizes to observed discharge to attempt to improve the volume of the snow pack. The first calibration will adjust parameters according to MODIS SCA. However, the first calibration does not address potential issues with volume of melt water. This calibration will perform this task by using the SACSMA discharge to adjust the SCF parameter in SNOW17, which will impact the amount of SWE accumulated in the the snow pack.

The third calibration was done independent of the first and second calibrations. The purpose of the calibration was to see if optimal performance of both SCA and snow melt volume could be obtained in one calibration. This calibration is similar to the first one in that the MAE objective function was used to evaluate modeled SCA from the SNOW17 against MODIS SCA. The three parameters from the first calibration (SI,MFMAX,PXTEMP), along with SCF were calibrated in one calibration run. The remaining SNOW17 parameters were taken from the CNRFC. To evaluate the impact on discharge, the SACSMA model was also run. All SACSMA parameters from the CNRFC were used. The goal of this calibration is to analyze whether parameters calibrated against MODIS data alone (i.e. without discharge observations) can improve model performance against operational parameters the NWS uses.

2.4 Model Evaluation

Output statistics were performed on modeled SCA from the SNOW17 and modeled discharge from the SACSMA. Average error statistics were computed over each elevation zone. Statistics computed using discharge were considered to represent the basin-wide model skill of the SNOW17 and SACSMA combined. Four main error statistics were computed for

both models: MAE (see eqn 2.1-2.3), Nash-Sutcliffe efficiency (NS), bias, and correlation coefficient:

$$\text{NS} = 1 - \frac{\frac{1}{n}\sum_{t=1}^{n}[d_t - o_t]^2}{\frac{1}{n}\sum_{t=1}^{n}(d_t - \bar{d}_t)} \quad (3.1)$$

$$\text{Bias} = \frac{1}{n}\sum_{t=1}^{n}(d_t - o_t) \quad (3.2)$$

$$\text{Correlation Coefficient} = \frac{\sum_{t=1}^{n}(d_t - \bar{d})(o_t - \bar{o})}{\sqrt{\sum_{t=1}^{n}(d_t - \bar{d})^2}\sqrt{\sum_{t=1}^{n}(o_t - \bar{o})^2}} \quad (3.3)$$

where d_t is observed discharge at timestep t, o_t is SACSMA discharge at timestep t, and n is the number of pixel cells in each elevation zone. For NS, values from 0.5-1.0 indicate optimal model performance, values from 0.0-0.5 indicate some model accuracy, while any values less than 0.0 indicate poor model performance. For optimal model performance, correlation coefficient values close to a value of one are desired and Bias values close to zero are desired.

CHAPTER 3: CALIBRATION FINDINGS

3.1 Comparison to Operational Lumped SNOW17

The SNOW17 and SACSMA were first run in lumped mode (2 elevation zones) using the CNRFC parameter values in order to provide a baseline for evaluation of the data, distributed model application, and calibrations conducted in this study. An initial model run was done using mean areal precipitation (MAP) and mean areal temperature (MAT) provided by the CNRFC. It should be noted that data associated with the last two years of the study were unavailable from the CNRFC. The CNRFC is still processing this data before it is released. This run was compared to a model run using MAP and MAT developed from the spatial temperature and precipitation data sets used in this study. Temperature and precipitation values were averaged across all grid cells within the upper and lower elevation zones. In addition, a third model run was conducted using a distributed version of the SNOW17 with a lumped version of the SACSMA with the CNRFC parameters. This third model run was done to compare how well the distributed version of the SNOW17 performs against the lumped SNOW17 since the calibrations were done using the distributed SNOW17.

In some years, MAE values were higher when using the lumped and distributed data created by this study compared to the CNRFC data (Table 3.1). For the entire period of study, MAE was 463.8 cfs using the CNRFC data, 479.8 cfs using the lumped data created for this study, and 493.9 cfs using the distributed model. This comparison is a check to see how reliable the temperature and precipitation data created holds up against data that has been quality-controlled and used extensively by the CNRFC. This comparison also provides

a method to identify any potential biases that may exist with the data created. Even though there are some discrepancies between the observed discharge and modeled discharge for the watershed, there is an overall good agreement between the data used in this study and the CNRFC data, providing a degree of confidence in the accuracy of the temperature and precipitation data used in this study.

Table 3.1: MAE values (cfs) for SACSMA discharge using the RFC data and the study data for March 1st-June 30th.

Version	2001	2002	2003	2004	2005	2006	2007	2008	2009	Mean
Lumped with RFC Data	430.0	272.0	363.6	295.3	969.9	705.5	210.4			463.8
Lumped with Study Data	415.9	345.3	568.9	257.0	1062.9	533.8	281.7	362.3	490.0	479.8
Distributed with RFC Parameters	327.9	395.6	512.9	334.3	1039.3	669.5	240.0	410.8	514.7	493.9

Correlation coefficient values also show overall agreement between the three models. Table 3.2 lists correlation coefficient values of the three models. Year by year performance between the two versions is split. However, the CNRFC data had a mean coefficient value very similar of 0.84 versus 0.81 using the lumped study data. The distributed data produced a mean value of 0.84, which matches the lumped CNRFC data.

Table 3.2: Correlation coefficient values for SACSMA discharge using RFC data and the study data for March 1st-June 30th.

Version	2001	2002	2003	2004	2005	2006	2007	2008	2009	Mean
Lumped with RFC Data	0.83	0.78	0.88	0.89	0.79	0.83	0.83			0.84
Lumped with Study Data	0.90	0.83	0.61	0.89	0.65	0.94	0.76	0.90	0.78	0.81
Distributed with RFC Parameters	0.90	0.79	0.69	0.95	0.69	0.91	0.82	0.90	0.93	0.84

Nash-Sutcliffe values were also in fair agreement between the three data sets. Table 3.3 lists the values for the three model versions for each water year. While the RFC data produced a value of 0.40, the lumped study data was fairly close with a value of 0.30, as well as the distributed study data with a value of 0.33.

Table 3.3: Nash-Sutcliffe Values for SACSMA discharge using the RFC data and the study area for March 1st-June 30th.

Version	2001	2002	2003	2004	2005	2006	2007	2008	2009	Mean
Lumped with RFC Data	-0.29	0.51	0.63	0.48	0.36	0.54	0.56			0.40
Lumped with Study Data	-0.20	0.54	0.15	0.55	0.18	0.80	0.14	0.12	0.43	0.30
Distributed with RFC Parameters	0.24	0.39	0.27	0.46	0.20	0.69	0.38	-0.14	0.46	0.33

Bias values also show agreement between the three model runs. Table 3.4 shows bias values for each data set. Like previous error statistics, model performance is split between the two versions for a majority of the years. However, the difference between the mean bias values is less than 30 cfs for all three models, demonstrating fairly good agreement between the two data sets.

Table 3.4: Bias values (cfs) for SACSMA discharge using the RFC data and the study area for March 1st-June 30th.

Version	2001	2002	2003	2004	2005	2006	2007	2008	2009	Mean
Lumped with RFC Data	-430.0	-188.0	-297.4	-281.6	-951.4	-550.0	-142.5			-405.8
Lumped with Study Data	-415.6	-136.6	-314.6	-246.2	-942.2	-474.6	-215.1	-362.3	-402.7	-390.0
Distributed with RFC Parameters	-323.2	-163.6	-339.5	-334.3	-967.1	-619.6	-204.8	-410.8	-511.7	-430.5

Figure 3.1 shows comparisons of modeled discharge from both lumped versions of the SACSMA model to observed values for the 2001-2007 water years from the April through June. For the most part, the time of peaks for both models is in fair agreement. One exception to this is with the 2007 water year, where the RFC model run tends to follow observed discharge during the month of May more accurately. The MAT and MAP files were analyzed to look for a potential cause of the discrepancy during the 2007 water year. It should be noted that comparisons are missing for the 2008 and 2009 water years because data from the CNRFC have not been processed for calibration purposes yet. Precipitation values provided by the RFC were significantly higher than the precipitation values of this study during the time period shown in Figure 3.1g. In addition, temperature values provided by the RFC were also higher than the temperature values provided by this study. Higher precipitation values in combination with higher temperature values will cause the model to produce more snow melt and surface runoff in the SACSMA and SNOW17 models. The combination of these two factors will lead to a higher modeled discharge for the time period being addressed.

Figure 3.2 shows comparisons of modeled discharge from the SACSMA, using both the lumped and distributed study data, to the observed discharge. While there are some differences in peak discharge during the 2001, 2007, and 2008 water years, the modeled discharge is very similar in magnitude and pattern. This suggests that the difference between using a lumped SNOW17 and distributed SNOW17 with CNRFC parameters is small enough that the distributed SNOW17 is close to the lumped SNOW17 using the CNRFC parameters. This can justify using the distributed SNOW17 in place of the lumped SNOW17 for comparisons to the calibrated model runs later on.

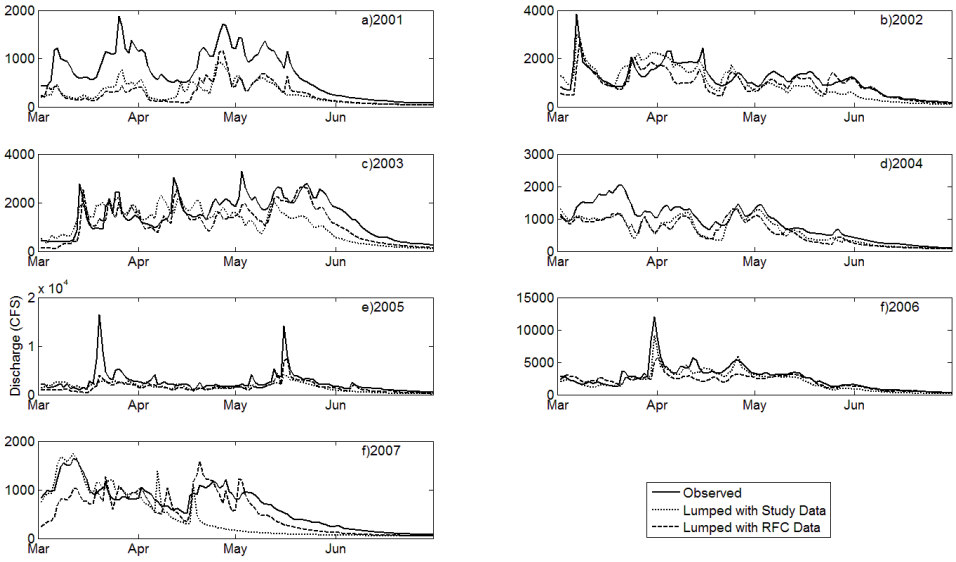

Figure 3.1: A comparison of SACSMA discharge to observed values for the March-June period for the 2001-2009 water years for a lumped version of SNOW17 using both the data created by this study and CNRFC data.

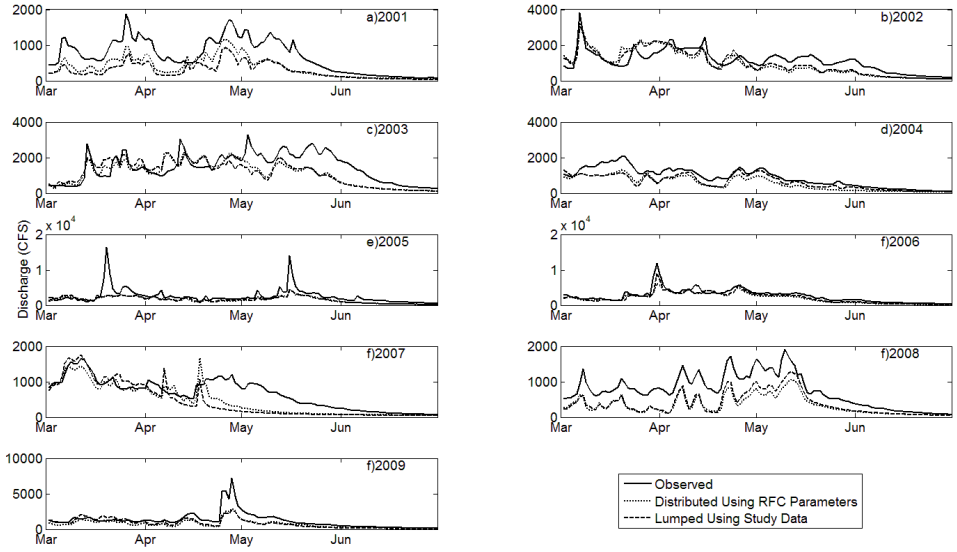

Figure 3.2: A comparison of SACSMA discharge to observed values for the March-June period for the 2001-2009 water years for a lumped and distributed version of the SNOW17 using the data created in this study.

3.2 Calibration Comparisons

Three versions of the SNOW17 were run in conjunction with the SACSMA model. Each version had a calibrated set of parameters (Tables 3.1-3.4). The methods of developing these parameters were described in section 2.3. Calibration model runs were compared to a distributed version of the SNOW17 ran with the SACSMA model using original CNRFC parameters. Analysis done on SCA output from the SNOW17 is presented in 3.2.1,and analysis on SACSMA discharge is presented in 3.2.2.

Looking at tables 3.5-3.7, one common theme between all three parameter value tables is the sudden shift in values from elevation zone three to elevation zone four. MFMAX drops from 3.09 in zone two to 0.53 in zone three, before jumping back up to 1.03 in zone four. PXTEMP drops from 3.00 in zone three to 1.23 in zone four. With the second calibration, SCF dropped from 2.0 in zone three to 0.50 in zone four. One potential reason behind this is the spatial distribution of temperature data that went into the SNOW17 calibrations. Monthly average temperature values were computed, for the entire period of study to look for any distinct patterns in the elevation zones. Outside of elevation zone four, the spatial temperature pattern across each individual elevation zone is somewhat homogenous (Figure 3.3). However, within elevation zone four, there is a higher spatial variability in average monthly temperature values when compared to the other elevation zones (Figure 3.3). This variability and shift may be a cause for the dramatic shift in parameter values.

Table 3.5: First set of calibrated SNOW17 parameters using MODIS SCA.

Parameter	Elevation Zone 1	Elevation Zone 2	Elevation Zone 3	Elevation Zone 4	Elevation Zone 5	Elevation Zone 6
SI	839.15	39.25	92.32	75.41	15.70	183.53
MFMAX	3.50	3.09	0.53	1.03	1.00	2.01
PXTEMP	0.50	3.00	3.00	1.23	2.83	0.79

Table 3.6: Second Set of calibrated SNOW17 parameters using SACSMA discharge.

Parameter	Elevation Zone 1	Elevation Zone 2	Elevation Zone 3	Elevation Zone 4	Elevation Zone 5	Elevation Zone 6
SCF	1.97	2.00	2.00	0.50	1.43	1.12

Table 3.7: Third set of calibrated SNOW17 parameters using MODIS SCA.

Parameter	Elevation Zone 1	Elevation Zone 2	Elevation Zone 3	Elevation Zone 4	Elevation Zone 5	Elevation Zone 6
SCF	0.50001	2.00	2.00	1.37	0.97	0.57
SI	737.70	37.22	158.18	80.27	15.04	103.52
MFMAX	3.50	3.11	1.21	1.34	0.96	0.98
PXTEMP	0.50	3.00	2.35	0.50	2.82	1.82

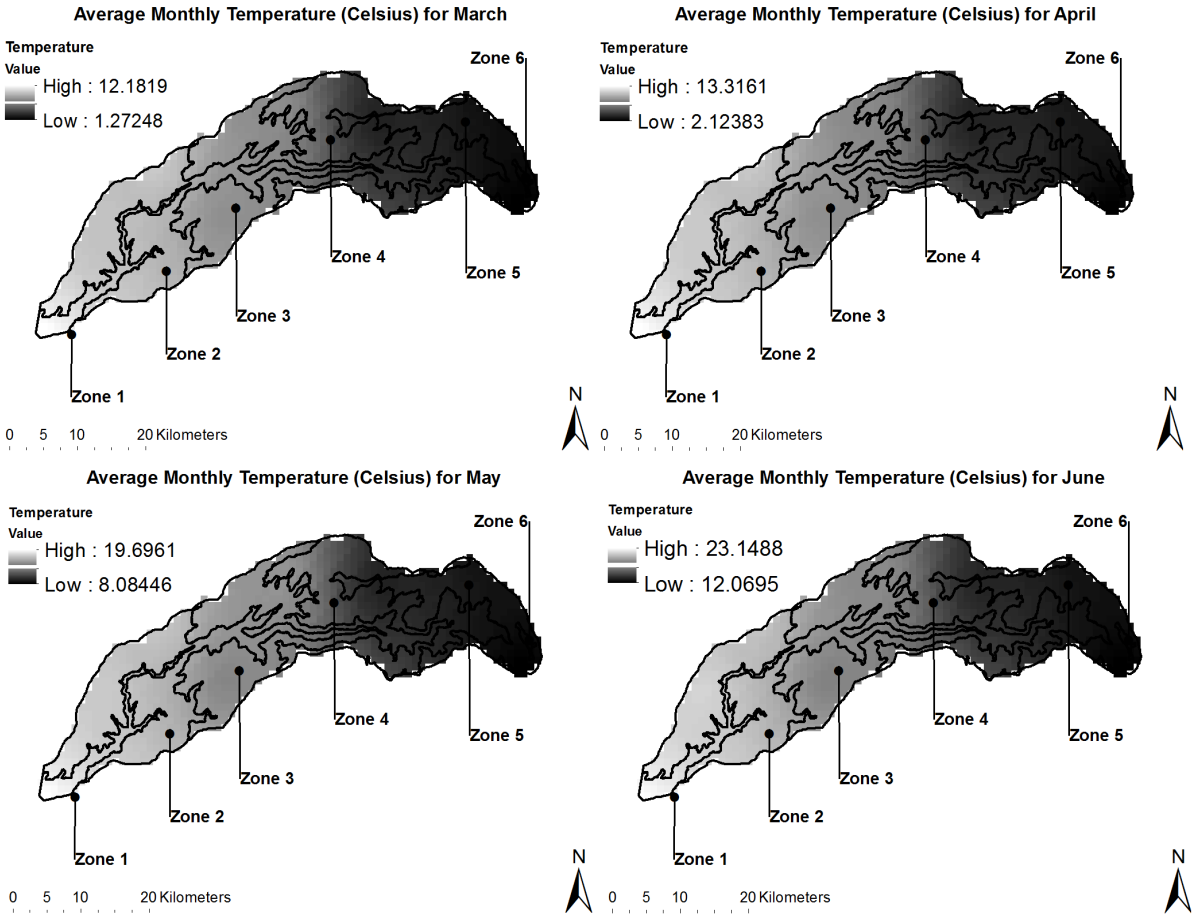

Figure 3.3: Monthly average temperature values across the watershed for March – June. Elevation zone boundaries are deonted with the solid black lines.

3.2.1 SCA Comparisons

Analysis of the SCA for each calibration run yields results that vary by elevation zone. MAE decreased for both the calibration and verification period for all three calibrations (Table 3.8). The largest improvement came from the third calibration, where MAE decreased by 0.8% for the calibration period and 1.1% for the verification period. Improvement is also present in the correlation coefficient values, which increased with all three calibrations for both the verification and calibration periods (Table 3.9). Correlation coefficient values were

the highest for the verification period of the third calibration with a value of 0.142. Nash-Sutcliffe values rose for the first and third calibrations, but values were still substantially below the optimal value of 0 (Table 3.10). This is most likely attributed to the highly variable nature of the snow cover extent in this elevation zone. A highly variable snow cover is more difficult for the model to accurately simulate, leading to a lower Nash-Sutcliffe value. Bias values decreased for all three calibrations for the entire period of study for the first elevation zone (Table 3.11). The third calibration saw the greatest reduction in bias values with bias being reduced from 12.4% to 0.5% for the verification period.

Analysis of the second elevation zone had mixed results. For the first calibration, MAE decreased by 0.9% and 0.7% for the calibration and verification periods (Table 3.8). However, for the second calibrations, MAE increased by 0.9% and 2.2% for both periods (Table 3.8). MAE decreased by 1.1% and 1.0% for the third calibration for calibration and verification periods (Table 3.8). For correlation coefficient, the only time of improvement occurred with the second calibration during the verification period, where values increased from 0.438 to 0.441 (Table 3.9). Nash-Sutcliffe values increased for the first and third calibrations, but decreased for the second calibration (Table 3.10). The greatest rise occurred with the third calibration as values increased from -40.4 to -24.5 for the calibration period and from -20.5 to -15.0 for the verification period (Table 3.10). Bias values showed a similar pattern with a decrease for the first and third calibrations, but an increase for the second calibrations (Table 3.11). The largest decreases occurred with the third calibration as values fell to 1.6% and 2.5% for the calibration and verification periods (Table 3.11). The increase in errors for the second calibration could be due to the second calibration being done using

SACSMA discharge as opposed to MODIS SCA. This would explain why the same decrease in errors weren't present with the independent third calibration.

For the third elevation, results were uniform across all three calibrations. MAE increased for all three calibrations, with the largest rise occurring with the second calibration during the calibration period (Table 3.8). Nash-Sutcliffe values decreased for all three calibrations, with the largest decreases also occurring with the second calibration during the calibration period (Table 3.10). Bias values increased for all three calibrations, with the largest increases occurring with the second calibration (Table 3.11). One exception to this pattern with the third elevation occurred with the correlation coefficient values. Correlation coefficient values increased for all three calibrations for both time periods (Table 3.9). The largest increases in correlation coefficient values occurred with the third calibration (Table 3.9). This would lead to conclusion that the calibrations were better able to reproduce the SCA depletion patterns, but not the magnitudes of the SCA values.

For the fourth elevation zone, the third calibration was the model run that saw the largest decrease in performance. MAE rose from 17.5% to to 23.8% for the calibration period and from 13.0% to 22.9% for the verification period with the second calibration model run (Table 3.8). A similar pattern emerged with the correlation coefficient values, Nash-Sutcliffe, and bias values (Table 3.9-3.11). This pattern could easily be attributed to reasons mentioned earlier regarding the nature of the second calibration.

For the fifth elevation zone, performance was degraded with all three calibrations. MAE values increased for all three model runs, with the largest increases occurring with the second calibration and the smallest increases occurring with the third calibration (Table 3.8). Correlation coefficient values decreased across all model runs as well, with the least amount

of decrease occurring with the third calibration (Table 3.9). Nash-Sutcliffe values followed a similar pattern with decreases across all model runs, with the least amount of change occurring with the third calibration (Table 3.10). Bias values increased for all calibration model runs, with the least amount increase occurring in the third calibration (Table 3.11).

The sixth elevation zone had mixed results from the various calibrations. With MAE, values decreased with the first two calibrations, but saw a slight increase during the verification period with the third calibration run (Table 3.8). Correlation coefficient values increased for the calibration period for the first two model runs. However, values decreased slightly for the verification periods for all three model runs, and the calibration period for the third model run (Table 3.9). A similar pattern occurred with Nash-Sutcliffe values, with the only improvement occurring during the calibration period for the first two model runs (Table 3.10). Bias values decreased for all three model runs, for all periods (Table 3.11). However, the magnitudes of the bias values didn't always decrease, as was the case with the third calibration model run (Table 3.11).

Although at times, there were mixed results from the calibration model runs, there were multiple elevation zones that did see improvement in SCA during the spring melt period. This was especially true for the first calibration, which saw the least number of instances where error increased. The third calibration had more mixed results, which could be as a result of trying to calibrate SCF, SI, MFMAX, and PXTEMP all at once. The second calibration saw the least amount decrease in error across the elevation zones, which could easily be as a result of the SACSMA discharge as opposed to MODIS SCA being used for calibration. These statistics support using MODIS SCA to improve SNOW17 parameters.

Table 3.8: SNOW17 SCA MAE (%) comparisons across the different calibrations for both the calibration and verification periods for March 1st – June 1st.

	RFC Parameters		1st Calibration		2nd Calibration		3rd Calibration	
Elevation Zone	Cal Period	Ver Period	Cal Period	Ver Period	Cal Period	Ver Period	Cal Period	Ver Period
1	1.3	1.7	8.0	1.0	1.1	1.4	5.0	0.6
2	4.1	4.5	3.2	3.8	5.0	6.7	3.0	3.5
3	14.0	9.6	27.7	21.5	51.7	40.3	28.7	23.3
4	17.5	13.0	17.5	15.0	23.8	22.9	15.7	14.7
5	16.6	12.7	28.5	25.7	32.0	27.6	20.1	19.4
6	18.6	15.0	12.5	13.8	13.5	15.1	16.9	17.7

Table 3.9: SNOW17 SCA Correlation coefficient comparisons across the different calibrations for both the calibration and verification perdiods for March 1st- June 1st.

	RFC Parameters		1st Calibration		2nd Calibration		3rd Calibration	
Elevation Zone	Cal Period	Ver Period	Cal Period	Ver Period	Cal Period	Ver Period	Cal Period	Ver Period
1	-.004	.122	.006	.137	.004	.130	.005	.142
2	.290	.438	.259	.357	.287	.441	.257	.346
3	.598	.681	.656	.735	.664	.738	.676	.749
4	.812	.859	.859	.852	.629	.684	.838	.840
5	.859	.897	.739	.682	.679	.649	.860	.812
6	.831	.882	.896	.851	.859	.831	.799	.797

Table 1.10: SNOW17 SCA Nash-Sutcliffe comparisons across the different calibrations for both the calibration and verification periods from March 1st – June 1st.

	RFC Parameters		1st Calibration		2nd Calibration		3rd Calibration	
Elevation Zone	Cal Period	Ver Period	Cal Period	Ver Period	Cal Period	Ver Period	Cal Period	Ver Period
1	-439.3	-57.3	-298.3	-35.9	-495.0	-81.8	-130.7	-11.4
2	-40.4	-20.5	-27.9	-17.6	-56.1	-43.8	-24.5	-15.0
3	-2.70	-.363	-11.2	-3.02	-32.8	-11.3	-11.6	-3.84
4	.367	.625	.294	.481	-.291	-.131	.388	.480
5	.577	.695	-.306	-.188	-0.61	-.342	.303	.321
6	.512	.654	.697	.607	.618	.528	.429	.337

Table 3.11: SNOW17 SCA Bias (%) comparisons across the different calibrations for both the calibration and verification periods from March 1st – June 1st.

	RFC Parameters		1st Calibration		2nd Calibration		3rd Calibration	
Elevation Zone	Cal Period	Ver Period	Cal Period	Ver Period	Cal Period	Ver Period	Cal Period	Ver Period
1	1.0	12.4	5.0	7.0	8.0	1.2	2.0	0.3
2	3.4	4.1	1.9	2.9	4.2	6.2	1.6	2.5
3	10.3	6.7	26.5	20.0	51.7	40.0	27.7	22.0
4	12.5	4.6	13.0	5.8	-14.7	-18.3	38.8	48..0
5	12.5	8.1	28.5	21.9	32.0	24.8	18.1	12.3
6	13.5	6.0	6.4	-0.2	-1.7	-7.1	-8.8	-11.1

Subjective analysis was also performed on the SCA output from the SNOW17 using spatial SCA images. Early on in the melt season, there may be very little difference between the various model runs (Figure 3.4). However, later in the melt period, especially May into June, the differences between the various model runs become quite apparent (Figure 3.5). Although there are still spatial errors with the distributed models, the first two calibrations do produce a more distributed pattern of SCA (Figure 3.5). However, with the third calibration, some of this detail is lost and the errors return (Figure 3.5). This is consistent with the statistical analysis that was performed above.

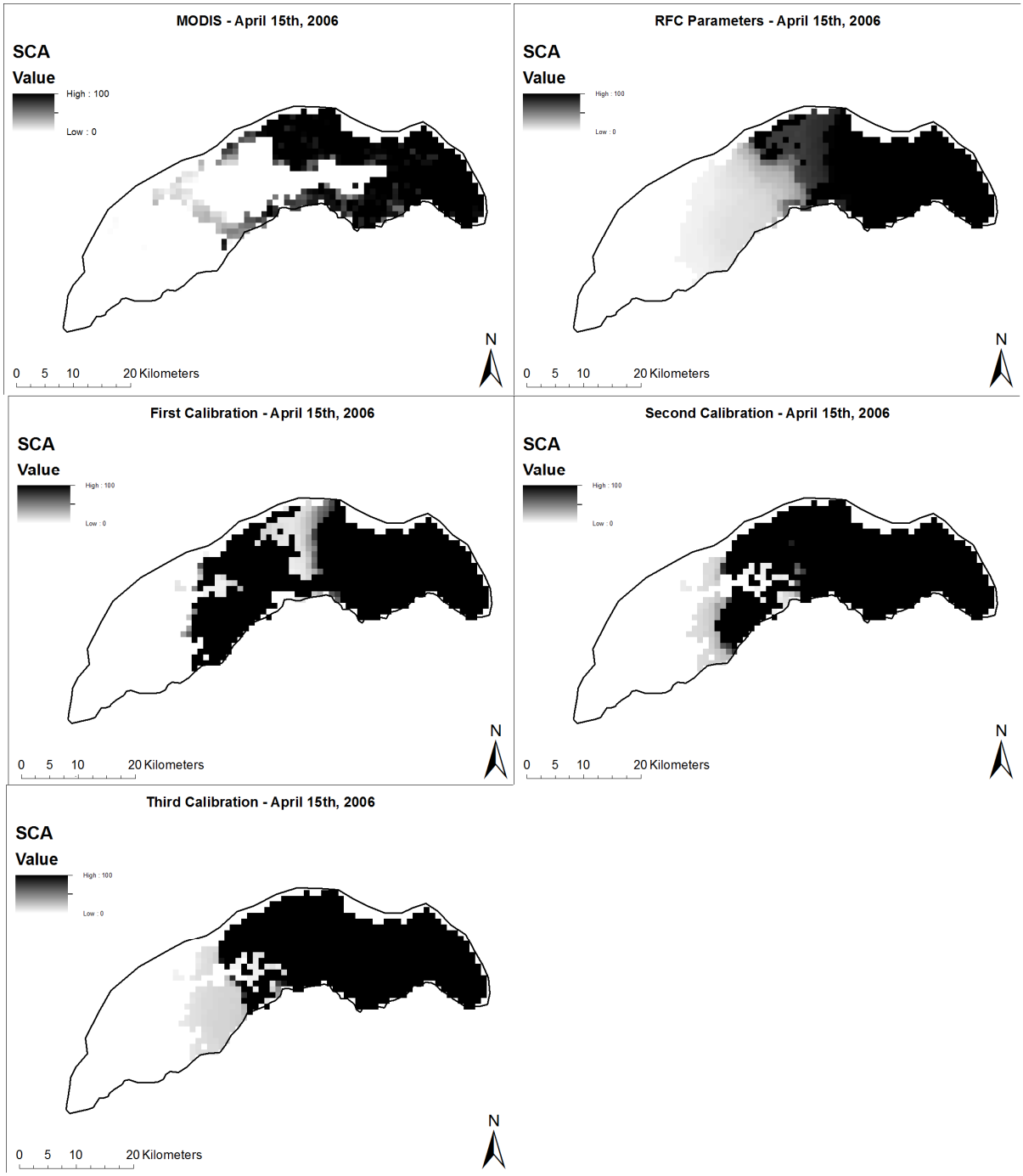

Figure 3.4: Distributed SCA for all calibrations compared to MODIS SCA and SNOW17 SCA with RFC parameters for April 15th, 2006.

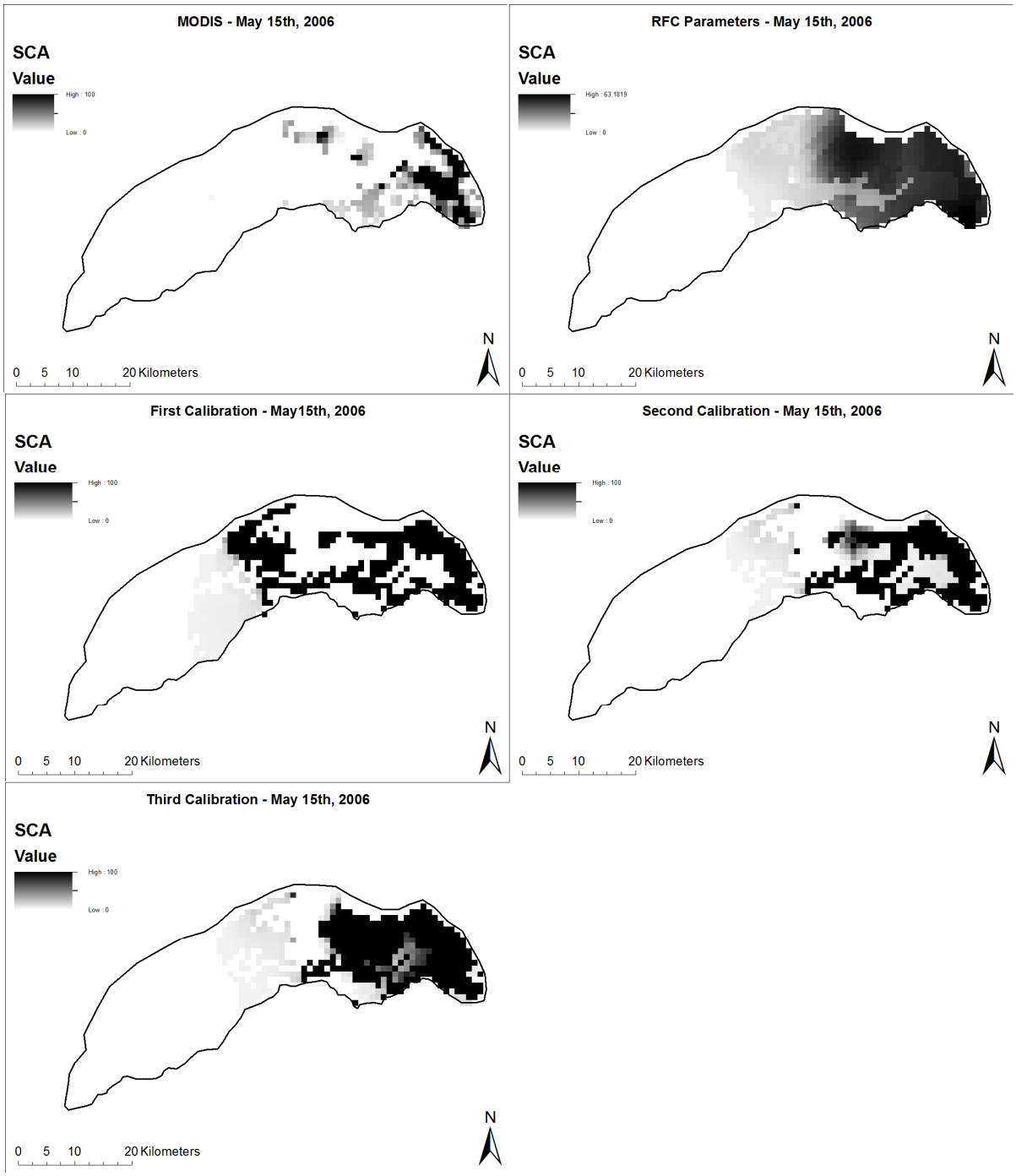

Figure 3.5: Distributed SCA for all calibrations compared to MODIS SCA and SNOW17 SCA with RFC parameters for May 15th, 2006.

3.2.2 SACSMA Discharge Comparisons

Analysis of SACSMA discharge shows improvement in discharge simulation for the spring melt season, especially with the first two calibrations. For the first two calibrations, MAE decreased across all years, with an exception of the 2007 water year (Table 3.12). The decrease in error was the largest for the 2008 water year when MAE decreased from 410.8 cfs to 174.4 cfs for the second calibration (Table 3.12). Another interesting note is that MAE decreased further from the first calibration to the second calibration for all years, except the 2007 and 2009 water years (Table 3.12). The overall mean in MAE decreased from 493.9 cfs to 398.6 cfs from the CNRFC parameters for the second calibration (Table 3.12). The further improvement with the second calibration should occur as the second calibration was done using observed discharge. However, the larger improvement with the first calibration seems to be a result of using MODIS SCA as opposed to observed discharge. The third calibration saw an increase in MAE during the melt season from 493.9 cfs to 589.7 cfs (Table 3.12). This is an interesting analysis because the third calibration was done in a similar fashion as the first calibration, with the addition of the SCF parameter. However, this resulted in a decrease in performance, where the first calibration saw an increase in performance. Another look at tables 3.5-3.7 shows that for the most part, the SI, MFMAX, and PXTEMP parameters are very similar between the first and third calibrations. However, the SCF parameter is different between the second and third calibrations. One hypothesis is that there is a physical process that is being picked up by the MODIS SCA that is translated through the SCF parameter in the second calibration to correct for volume of snow melt occurring.

Correlation coefficient values were mixed for the different calibrations. The largest decreases in values occurred with the third calibration as values decreased from 0.84 to 0.74 (Table 3.13). The first and second calibrations saw mixed results with the first calibration seeing an increase for three years, and a decrease for five years (Table 3.13). The second calibration saw an increase in correlation coefficient values for five years and a decrease for four years (Table 3.13). For the overall mean, there was only a difference of 0.02 between the CNRFC parameter run and the first and second calibration model runs, while the third calibration saw a decrease (Table 3.13). A decrease in MAE values, coupled with little change in correlation coefficient values for the first and second calibrations translates to a shift in the simulated discharge closer to the observed without a significant change in the pattern.

Nash-Sutcliffe values for the three calibrations followed a pattern similar to MAE. For the first two calibrations, with the exception of the 2002 and 2008 water years, saw an increase in values (Table 3.14). The third calibration saw a decrease in values for seven of the nine water years (Table 3.14). For the overall mean of all years, the values increased for the first two calibrations, while decreasing for the third calibration run (Table 3.14).

Bias values decreased in magnitude for all three calibrations for all years except 2002 (Table 3.15). This was especially true for the second calibration, where the overall mean was only 7.2 cfs (Table 3.15). As opposed to the previous three statistics, magnitude of bias error values showed improvement even with the third calibration (Table 3.15).

Table 3.12: SACSMA MAE (cfs) comparisons across the different calibrations for March 1st – June 30th.

Version	2001	2002	2003	2004	2005	2006	2007	2008	2009	Avg
RFC Pars	327.9	395.6	512.9	334.3	1039.3	669.5	240.0	410.8	514.7	493.
1st Cal	218.4	401.2	457.6	205.8	895.3	672.3	324.5	180.6	278.6	403.
2nd Cal	182.5	385.0	436.5	193.2	892.7	538.7	430.8	174.4	353.2	398.
3rd Cal	360.5	796.6	617.3	477.1	974.5	890.7	428.6	341.6	420.3	589.

Table 3.13: SACSMA Correlation coefficient comparisons across the different calibrations for March 1st – June 30th.

Version	2001	2002	2003	2004	2005	2006	2007	2008	2009	Avg
RFC Pars	0.90	0.79	0.69	0.95	0.69	0.91	0.82	0.90	0.93	0.84
1st Cal	0.85	0.82	0.73	0.94	0.57	0.78	0.82	0.94	0.89	0.82
2nd Cal	0.92	0.85	0.77	0.97	0.55	0.84	0.83	0.88	0.81	0.82
3rd Cal	0.78	0.75	0.60	0.91	0.55	0.78	0.79	0.71	0.81	0.74

Table 3.14: SACSMA Nash-Sutcliffe comparisons across the different calibrations for March 1st – June 30th.

Version	2001	2002	2003	2004	2005	2006	2007	2008	2009	Avg
RFC Pars	0.24	0.39	0.27	0.46	0.20	0.69	0.38	-0.14	0.46	0.33
1st Cal	0.59	0.14	0.46	0.72	0.24	0.58	0.05	0.75	0.73	0.47
2nd Cal	0.72	0.16	0.56	0.79	0.26	0.70	-0.74	0.74	0.63	0.42
3rd Cal	-0.07	-1.88	0.08	-0.04	0.26	0.45	-1.23	-0.00	0.63	-0.2

Table 3.15: SACSMA Bias (cfs) comparisons across the different calibrations for March 1st – June 30th.

Version	2001	2002	2003	2004	2005	2006	2007	2008	2009	Avg
RFC Pars	-323.2	-163.6	-339.5	-334.3	-967.1	-619.6	-204.8	-410.8	-511.7	-431
1st Cal	-130.7	203.5	-114.5	36.4	-601.7	-141.3	-15.5	-135.2	-212.8	-124
2nd Cal	83.2	341.6	2.9	82.1	-456.7	5.3	186.8	-30.4	-151.1	7.2
3rd Cal	109.3	431.5	55.2	209.8	-418.0	117.6	97.0	47.2	-150.0	55.5

Subjective analysis of the SACSMA discharge from the various calibration model runs can be done using figures 3.6-3.8, which shows hydrographs from each water year for

the spring melt period. For the first calibration, there are several periods where the modeled discharge for the calibrated model was much closer to the observed values when compared to the model using the CNRFC parameters (Figure 3.6). This is especially true for the 2008 water year, where modeled discharge is much closer to observed values than modeled discharge using CNRFC parameters. This matches up with statistics mentioned previously. There are some periods where the calibrated model run over estimated discharge compared to with the original CNRFC parameters, especially with the 2002 and 2007 water years (Figure 3.6). These also happen to be the years with the least amount of improvement with the error statistics.

With the second calibrated parameter set, the appearance of the hydrographs is similar to the first set of calibrated parameter values (Figure 3.7).There are a few peaks in 2002 that are closer to the observed values with the second calibrated parameter set (Figure 3.7). Modeled discharge went up even further during the first half of the melt period for the 2007 water year, which is a decrease in performance. Outside of those areas, the overall appearance of the modeled hydrographs does not appear to have changed much from the first set of calibrated parameters (Figure 3.7). This aligns with the error statistics in that error values did not change much from the first calibration to the second calibration, although there was some improvement.

With the third calibration, the appearance of the modeled hydrograph seems significantly altered from the first two calibrations (Figure 3.8). The overestimation of discharge that was present in the first two calibrations seems exagerated with the third calibration (Figure 3.8). Overall, the appearance seems to suggest an actual decrease in

performance when compared to the use of the original CNRFC parameters, which agrees with statistical analysis provided earlier (Figure 3.8).

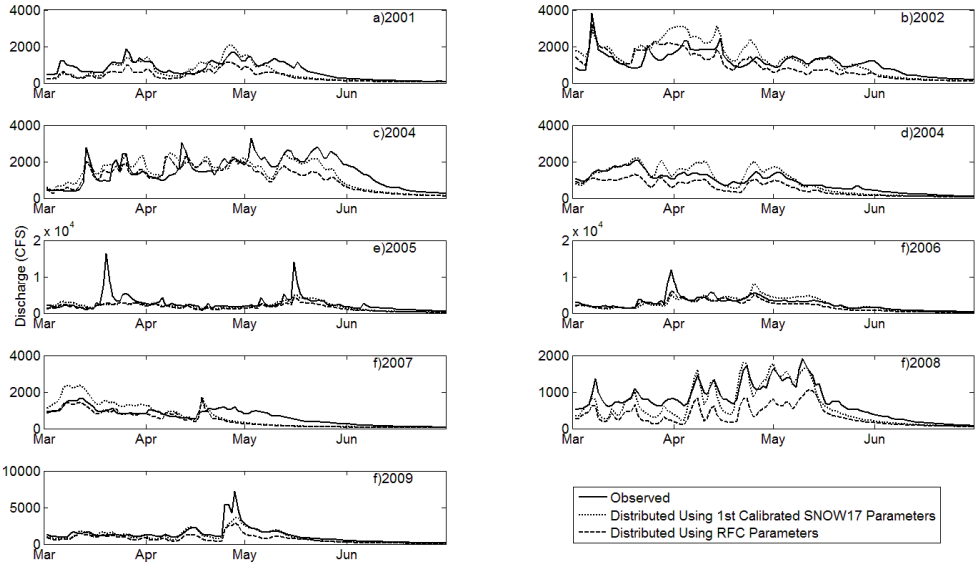

Figure 3.6: Comparison of SACSMA discharge for the verification period using the first SNOW17 calibration.

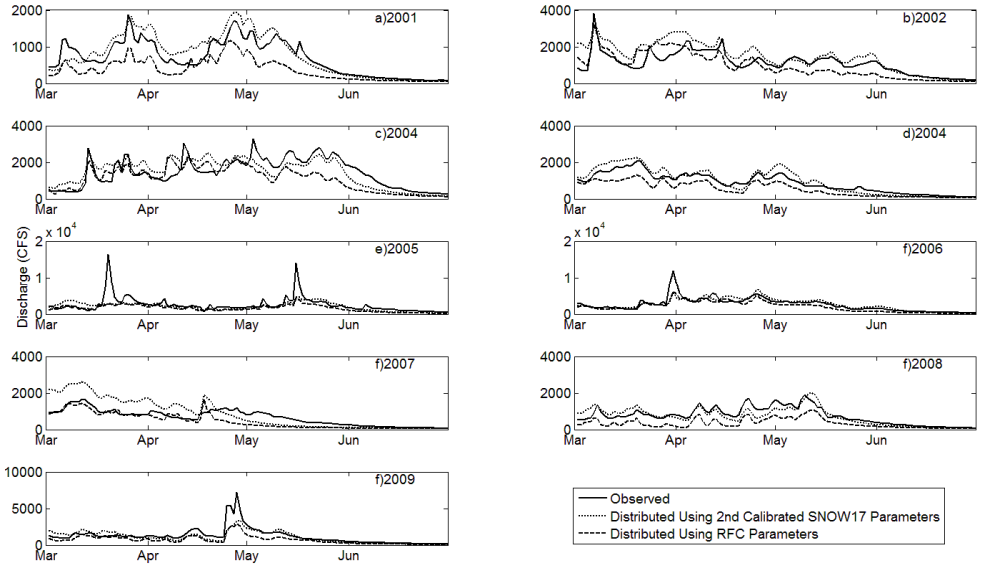

Figure 3.7: Comparison of SACSMA discharge for the verification period using the second SNOW17 calibrated parameters.

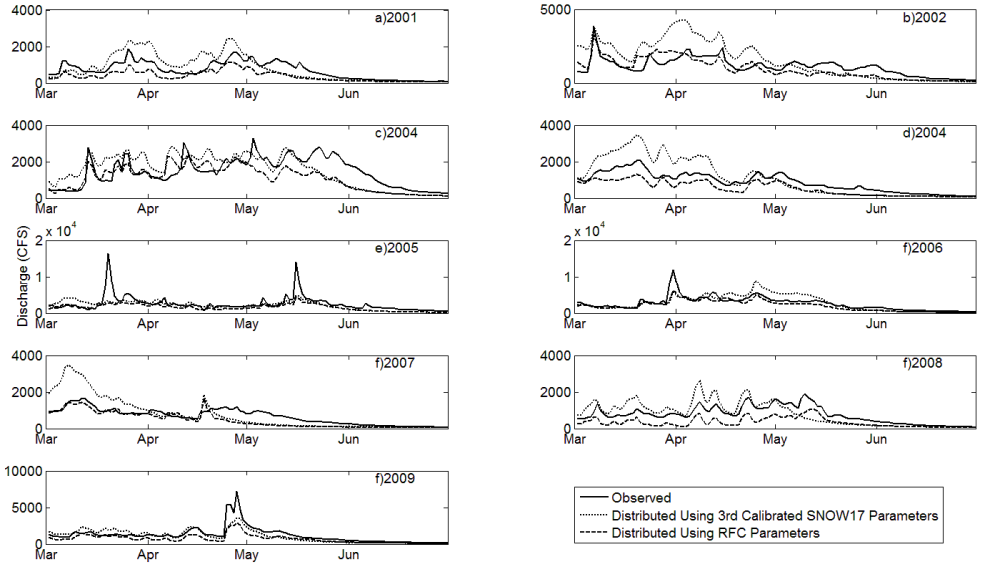

Figure 3.8: Comparison of SACSMA discharge for the verification period using the third SNOW17 calibrated parameters.

CHAPTER 4: ALBEDO RESULTS

4.1 Albedo Testing

The MODIS snow albedo product was tested as input to the modified SNOW17, which considers the snow energy balance. The hypothesis for this part of the study was that the MODIS albedo product would aid the modified SNOW17 model by creating a more physically-based energy balance at the snowpack surface. When the modified SNOW17 is run in conjunction with the SACSMA model, the improved snow melt simulation would result in a more accurate streamflow discharge.

Parameters provided by the CNRFC were used in the model runs (see tables 2.4 and 2.7). MODIS snow albedo was used directly in the model for the energy balance computations. Both the SNOW17 and SACSMA models were evaluated using several error statistics for both SNOW17 SCA and SACSMA discharge. The first three calibrations previously analyzed using the SNOW17 were included in this evaluation to see if the modified SNOW17 could improve upon the calibrations. The period of analysis was chosen as March 1st – June 1st for each water year of the study. This was done to focus on the spring period when most snow ablation occurs across the watershed. SNOW17 SCA was averaged for each of the six elevation zones and compared to an average MODIS SCA for each elevation zone. SACSMA discharge was compared to observed discharge at the outlet of the watershed.

Table 4.1 lists MAE values for each elevation zone using the energy balance SNOW17 along with the other versions of the SNOW17 analyzed earlier in this study. Values were fairly close to the other versions for most elevation zones, except with the third

and sixth zone. However, for most elevation zones, the MAE values were all higher than the other model runs, showing an overall decrease in model performance. This was especially true in elevation zones three and six where values rose significantly.

Table 4.1: SCA MAE (%) values for each elevation zone from March 1st - June 1st for the 2001-2009 water years.

Elevation Zone	Distributed with RFC Parameters	Distributed with 1st Calibration	Distributed with 2nd Calibration	Distributed with 3rd Calibratioin	Modified SNOW17
1	1.5	0.9	1.3	0.6	0.9
2	4.4	3.5	6.0	3.3	11.4
3	11.6	24.2	45.4	25.7	35.3
4	15.0	16.1	23.3	15.1	15.4
5	14.5	26.9	29.5	19.7	20.4
6	16.6	13.2	14.0	17.4	40.0

Table 4.2 lists the Nash-Sutcliffe values for each elevation zone with the same approach of modeling. The majority of the elevation zones had values lower than the calibrated versions, with a few exceptions. The 2nd calibration experienced lower values for all elevation zones, except the upper most zone. Looking back at table 4.1, some of the MAE errors were also higher for the 2nd calibration. These issues may be due to the correction of the SCF parameter due to the SACSMA discharge. Outside of the 2nd calibration, the majority of the other model run performed better overall with respect to Nash-Sutcliffe values.

Table 4.2: Nash-Sutcliffe values for each elevation zone from March 1st - June 1st for the 2001-2009 water years.

Elevation Zone	Distributed with RFC Parameters	Distributed with 1st Calibration	Distributed with 2nd Calibration	Distributed with 3rd Calibbration	Modified SNOW17 with MODIS Albedo
1	-227.1	-152.5	-265.4	-64.4	-107.5
2	-30.5	-22.1	-49.3	-19.2	-152.8
3	-1.40	-6.67	-20.9	-7.28	-12.3
4	0.51	0.40	-0.20	0.44	0.43
5	0.64	-0.24	-0.46	0.31	0.23
6	0.59	0.65	0.57	0.38	-0.89

Table 4.3 lists bias values for each elevation zone compared to other versions of the SNOW17. For the first three elevation zones, bias values are similar in magnitude than the other model versions. The upper three elevation zones have a negative bias compared to mostly positive bias for the other model versions. This suggests that the modified SNOW17 is melting snow too quickly, resulting in a negative bias. It was noted that MODIS snow albedo values were significantly lower than using an age-decay function to compute albedo. A lower albedo value will result in much quicker melt, resulting in a lack of SCA.

Table 4.3: Bias (%) values for each elevation zone from March 1st- June 1st for the 2001-2009 water years.

Elevation Zone	Distributed with RFC Parameters	Distributed with 1st Calibration	Distributed with 2nd Calibration	Distributed with 3rd Calibration	Modified SNOW17 with MODIS Albedo
1	1.3	0.6	1.0	0.3	0.6
2	3.8	2.4	5.3	2.1	11.2
3	8.3	22.9	45.2	24.5	34.6
4	8.1	9.0	-16.7	43.9	-1.1
5	8.3	24.8	28.0	14.9	-8.7
6	9.3	2.7	-4.7	-10.1	-35.7

Table 4.4 lists correlation-coefficient values for each elevation zone compared to other versions of the SNOW17. Performance using this statistic was similar than the Nash-Sutcliffe values. The only model version that seems to show some performance similar or worse than the MODIS albedo is calibration two. The main issues with the second calibration seem to lie within elevation zones four and five. Once again, this could be due to some correction being done by the SCF parameter, leading to an increased SCA error. However, elevation zone seemed to perform poorly using the MODIS albedo product. The first three elevation zones saw performance similar across all model versions.

Table 4.4: Correlation-coefficient values for each elevation zone from March 1st - June 1st for the 2001-2009 water years.

Elevation Zone	Distributed with RFC	Distributed with 1st Calibration	Distributed with 2nd Calibration	Distributed with 3rd Calibration	Modified SNOW17 with MODIS Albedo
1	0.07	0.09	0.08	0.09	0.08
2	0.37	0.31	0.37	0.31	0.38
3	0.64	0.70	0.71	0.72	0.65
4	0.84	0.86	0.66	0.84	0.80
5	0.88	0.71	0.66	0.83	0.71
6	0.86	0.87	0.84	0.80	0.49

In addition to SCA, modeled discharge from the SACSMA was analyzed to address model performance. Figures 4.1 and 4.2 show SACSMA discharge compared to other model versions. The modeled discharge that relied on a MODIS snow albedo performed much worse than other versions of the SNOW17 during the major snow ablation period. Most of the time, SACSMA discharge is much lower than the other model versions, suggesting that melt is occurring in the SNOW17 earlier and more quickly. This is another supporting argument that MODIS snow albedo may be too low, leading to an earlier onset of melting.

Analysis of the modified SNOW17 with MODIS snow albedo seems to suggest more work is needed to improve the albedo product before it is used in an energy-balance snow melt model. This can be especially true in watersheds such as the North Fork of the American River, where dense forest canopies can have a significant impact on the satellite's ability to measure albedo. With MODIS snow albedo values too low, more energy is going into the snowpack, leading to an earlier onset of melt. An earlier onset of melt will decrease model performance during snow ablation in the spring time, which is reflected in the statistics computed. Another future test could be applying the MODIS snow albedo to areas with little or no forest canopies. In these areas, a more comprehensive analysis can be done on the modified SNOW17 to test the applicability of an energy-balance snow melt model.

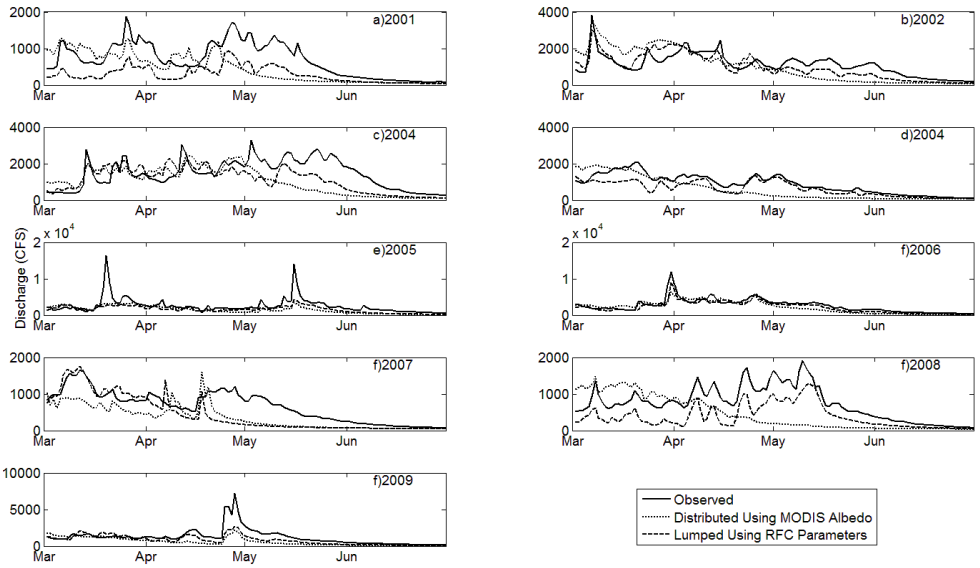

Figure 4.1: A comparison of SACSMA discharge using a lumped SNOW17 version with RFC parameters versus using a distributed energy balance version of SNOW17 with calibrated parameters for the 2001 through 2009 water years.

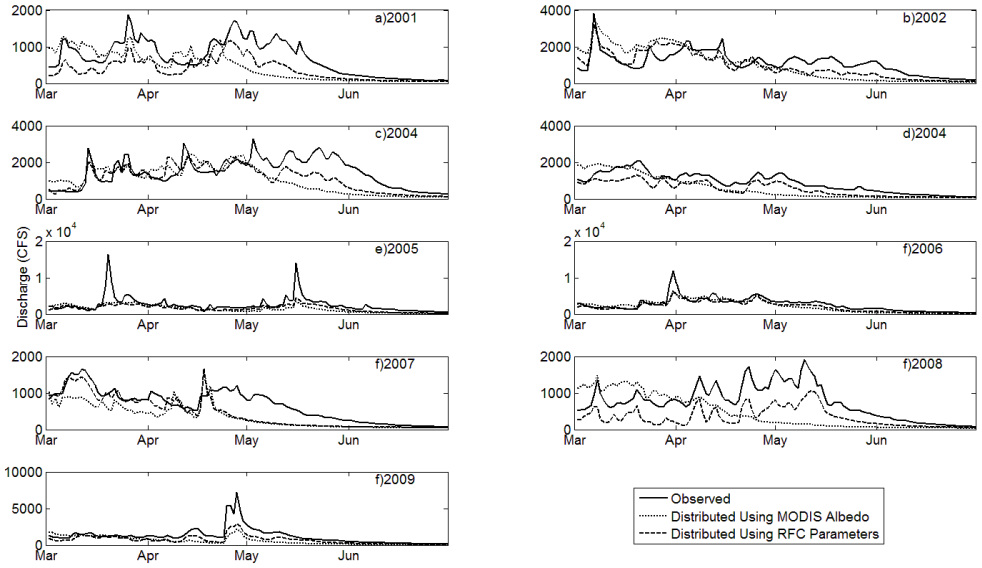

Figure 4.2: A comparison of SACSMA discharge using a distributed SNOW17 version with RFC parameters versus using a distributed energy balance version of SNOW17 with calibrated parameters for the 2001 through 2009 water years.

CHAPTER 5: CONCLUSIONS

5.1 Major Findings

During this study, a multi-step calibration (first and second calibration) and a single-step calibration (third calibration) approach were developed and tested for the SNOW17 and SACSMA models. The calibrations use MODIS SCA to optimize select snow model parameters that are traditionally calibrated using observed streamflow discharge. The calibrations were done using four years of MODIS and streamflow data. Five years were used for the verification period. Key parameters that have a major impact on snow ablation in the SNOW17 were chosen for calibration, holding all other parameters constant at the values provided by the CNRFC. In addition, MODIS snow albedo data was tested using a modified version of the SNOW17 to account for energy exchanges that occur at the snow pack surface. This study was performed for the North Fork of the American River basin in the Sierra Nevada Mountains in California.

The findings of this study are as follows:

(1) A multi-step approach utilizing both MODIS SCA and observed streamflow discharge produced improvement in simulated streamflow for the spring melt period, which runs from March 1st – June 30th. MAE decreased from 493.3 cfs using CNRFC parameters to 403.8 cfs in the first step of the calibration, and 398.6 cfs in the second calibration.

(2) Correlation coefficient values only changed by 0.02 from using the CNRFC parameters to the first and second calibration. This is an indication that the patterns of the discharge were not altered, but the overall mean error values was reduced.

(3) Nash-Sutcliffe values increased from 0.33 using the CNRFC parameters to 0.47 and 0.42 using the first and second calibrations. This is another indication that the model performance is improved using the multi-step calibration optimization.

(4) Overall bias values were reduced from -430.5 cfs using the CNRFC parameters to -123.5 cfs using the first calibration and 7.2 cfs using the second calibration.

(5) After testing a single step calibration routine, it was determined that optimizing the four SNOW17 parameters to MODIS SCA alone does not improve model performance nearly as much as the multi-step approach. This could be because SCA does not contain useful information about accumulated snow water equivalent to allow identification of the SCF parameter. There could also be parameter interactions between SCF, SI, MFMAX, and PXTEMP leading to a poorer approximation of these parameters when they are lumped together in one calibration

(6) The use of MODIS albedo in a heavily forested region yields little or no improvement in simulated SCA or SACSMA discharge using a modified version of the SNOW17.

5.2 Future Work

Future work should explore a potential three-step calibration approach, where the third approach would be calibrating key SACSMA parameters to stream flow discharge as the last calibration step once the SNOW17 parameters are calibrated. Other areas of future work include using the satellite data as direct forcing in the models, or utilizing a data

assimilation approach to update model states to better match satellite data. Additional testing of this technique can be applied to watersheds of varying geographic and atmospheric conditions. Another area of testing could be using multiple datasets to force the SNOW17 to test the sensitivity of the forcing data.

REFERENCES

Anderson, E. A. (1973), National Weather Service River Forecast System-Snow Accumulation and Ablation Model, NOAA Technical Memorandum: NWS Hydro-17, U.S. National Weather Service.

Andreadis, K. M., D. P. Lettenmaier (2005), Assimilating remotely sensed snow observations into a macroscale hydrology model, *Advances in Water Resources*, 29, 872-886.

Bitner, D., T. Carroll, D. Cline, and P. Romanov (2002), An Assessment of the differences between three satellite snow cover mapping techniques, *Hydrological Processes*, 16, 3723-3733.

Brazil, L. E., and M. D. Hudlow (1981), Calibration procedures used with the National Weather Service Forecast System. In *Water and Related Land Resources*. Pp 457-466.

Brubaker, K., A. Rango, and W. Kustas (1996), Incorporating radiation inputs into the snowmelt runoff model, *Hydrol. Processes*, 10, 1329-1343.

Burnash, R. J. C., R. L. Ferral, and R. A. McGuire, (1973), A generalized streamflow simulation system: Conceptual models for digital computers, National Weather Service, NOAA, and the State of California Department of Water Resources technical report: Joint Federal-State River Forecast Center.

Daly C., W. Gibson, M. Doggett, and J. Smith (2010), Near-real-time monthly high-resolution precipitation climate data set for the conterminous United States, *PRISM Group at Oregon State University.*, http://prism.oregonstate.edu.

Dery, S., V. V. Salomonson, M. Stieglitz, D. K. Hall, and I. Appel (2005), An approach to using snow areal depletion curves inferred from MODIS and its application to land surface modeling in Alaska, *Hydrological Processes*, 19, 2755-2774.

Dettinger, M. D., D. R. Cayan, M. K. Meyer, and A. E. Jeton (2004), Simulated hydrologic responses to climate variations and change in the Merced, Carson, and American River Basins, Sierra Nevada, California, 1900-2099, *Climate Change*, 62(1-3), 283-317.

Duan, Q., V. K. Gupta, and S. Sorooshian (1992), Effective and efficient global optimization for conceptual rainfall-runoff models. *Water Resour. Res.*, 28, 1015-1031.

Elder, K., J. Dozier, and J. Michaelsen (1991), Snow Accumulation and Distribution in an Alpine Watershed, *Water Resources Research*, 27(7), 1541-1552.

Franz, K. J., (2006). Characterization of the comparative skill of conceptual and physically-based snow models for streamflow prediction. Ph.D. Dissertation, University of California, Irvine.

Franz, K. J., P. Butcher, N. K. Ajami (2010), Addressing snow model uncertainty for hydrologic prediction, *Advances in Water Resources*, 33, 820-832.

Goodell, B.C. (1966), Snowpack management for optimum water benefits. In *ASCE Water Resources Engineering Conference Preprint 379*. Denver, CO.

Hogue, T. S., S. Sorooshian, H. Gupta, A. Holtz, and D. Braatz (2000), A multistep automatic calibration scheme for river forecasting models, *Journal of Hydrometeorology*, 1, 524-542.

Klein, A. G., and J. Stroeve (2002), Development and validation of a snow albedo algorithm for the MODIS instrument, *Annals of Glaciology*, 34. 45-52.

Klein, A. G. (2003), Determination of broadband albedos of partially snow-covered sites for validation of MODIS snow albedo retrievals. In *60th Eastern Snow Conference*. Sherbrooke, Quebec, Canada.

Klein, A. G., and A. C. Barnett (2003), Validation of daily MODIS snow cover maps of the Upper Rio Grande river basin for the 2000-2001 snow year, *Remote Sensing of Environment*, 86, 162-176.

Knowles, N., M. D. Dettinger, and D. R. Cayan (2006), Trends in snowfall versus rainfall in the Western United States, *Journal of Climate*, 19, 4545-4559.

Maurer, E. P., J. D. Rhoads, R. O. Dubayah, and D. P. Lettenmaier (2003), Evaluation of the snow-covered area data product from MODIS, *Hydrological Resources*, 17, 59-71.

Messinger F., G. DiMego, E. Kalnay, K. Mitchell, P. C. Shafran, W. Ebisuzaki, D. Jovic, J. Woollen, E. Rogers, E. H. Berbery, M. B. Ek, Y. Fan, R. Grumbine, W. Higgins, H. Li, Y. Lin, G. Manikin, D. Parrish, and W. Shi (2005), North American regional reanalysis, *Bulletin of American Meteorological Society*, 87, 343-360.

Miller, N. L., K. E. Bashford, and E. Strem (2003), Potential impacts of climate change on California hydrology, *Journal of the American Water Resources Association*, 39(4), 771-784.

Molotch, N. P., R. C. Bales (2006), Comparison of ground-based and airborne snow surface albedo parameterizations in an alpine watershed: Impact on snowpack mass balance, *Water Resources Research*, 42, 1-12.

NWS (2004), The National Weather Service River Forecast System User's Manual, available online at http://www.nws.noaa.gov/ohd/hrl, referenced version was downloaded on September 17th, 2007.

Shamir, E., and K. P. Georgakakos (2006), Estimating snow depletion curves for American River basins using distributed snow modeling, *Journal of Hydrology*, 334, 162-173.

Steppuhn, H. (1981), Snow and Agriculture. In *Handbook of Snow: Principles, Processes, Management and Use*, ed. D. M. Gray and D. H. Male. Toronto: Pergamon Press, pp. 60-125.

Stewart, I. T. (2009), Changes in snowpack and snowmelt runoff for key mountain regions, *Hydrological Processes*, 23, 78-94.

Storr, D. (1967), Precipitation variations in a small forest watershed, *Proceedings of the 35th Annual Western Snow Conference*, pp. 11-16.

Stroeve, J. C., J. E. Box, and T. Haran (2006), Evaluation of the MODIS (MOD10A1) daily snow albedo product over the Greenland ice sheet, *Remote Sensing of the Environment*, 105, 155-171.

Tekeli, A. E., A. Sensoy, A. Sorman, Z. Akyurek, and U. Sorman (2006), Accuracy assessment of MODIS daily snow albedo retrievals with in situ measurements in Karasu basin, Turkey, *Hydrological Resources*, 20, 705-721.

Wilby, R. L., and M. D. Dettinger, (2003), Streamflow changes in the Sierra Nevada, California, simulated using a statistically downscaled general circulation model scenario of climate change, *Advances in Global Change Research*, 6, 99-121.

ACKNOWLEDGEMENTS

I would like to thank my advisor, Dr. Kristie Franz for presenting me the opportunity to be part of her research group. It has been an honor to work under her guidance, and her support has helped me build a foundation of research skills and abilities. Without her support, I would not have acquired the knowledge to move me to the next steps in my life.

I would like to thank Dr. Brian Hornbuckle and Dr. William Gutowski for serving on my master's committee and taking the time to read and critique this thesis.

I would like to thank my office mates Scott Lincoln, Angela Bowman, and Chris Karstens for general advice on various topics.

I would also like to thank Daryl Herzman and Phillip Butcher for research advice and technical knowledge.

Financial support for this work is provided by Iowa State University and partial funding provided by NASA Grand #NNX08AH18G are greatly appreciated.